CSE - 190014

AN ALCOHOL SENSING DISPLAY WITH ALARM PROJECT



A Project

By

Md. Moniruzzaman
ID: CSE1502005004

K.M. Abu Sayeed
ID: CSE1502005022

Simul Parvej
ID: CSE1502005015

Ruman Mollah
ID: CSE1502005037

Abdilahi Mohamed
ID: CSE1502005035

PRESENTED TO

Md. Naderuzzaman
Asst. Professor , Dept. Of CSE
Sonargaon University , Dhaka

Department of Computer Science and Engineering
Sonargaon University (SU), Dhaka

May 2019

DECLARATION

Supervisor Declaration

I confirm that, the best of my knowledge. The research was carried out and the project was prepared under my direct supervisor. It represents the original research work of the candidates. The contribution made to the research by me and I have read this work and in my opinion this work is adequate in terms of scope and quality for the purpose of awarding the degree of Bachelor o science in Computer Science and Engineering. This is certifying that below statement made by the candidates is correct and true to the best of my knowledge.

.....

Md. Naderuzzaman

Asst. Professor, Dept. Of CSE

|Sonargaon University, Dhaka

Candidate's Declaration

We hereby declare that the work which is being presented in the project entailed, " An Alcohol Sensing Display with Alarm Project"

In partial fulfillment of the requirements of the award of degree of bachelor of science on Computer Science and Engineering Submitted to the department of Computer and Engineering of Sonargaon University, Dhaka is an authentic record of our carried out under the supervision of Asst. Professor MD. Naderuzzaman during the session 2018-2019.

The matter presented in this thesis has not been submitted for the award of any other degree of this or any other university.

.....

Md. Moniruzzaman
ID: CSE1502005004

.....

K.M. Abu Sayeed
ID: CSE1502005022

.....

Simul Parvej
ID: CSE1502005015

.....

Ruman Mollah
ID: CSE1502005037

.....

Abdilahi Mohamed

ID: CSE1502005035

Acknowledgments

I would like to express my sincere gratitude and appreciation to my supervisor, Professor Andreas Mandelis, for his dedication, invaluable guidance, support, and expertise throughout my thesis and for giving me a great research opportunity. I would also like to thank my thesis committee members, Professor David Sinton and Professor Tom Chau, for their inputs and insights during my M.H.Sc program.

In addition, I would like to thank all the lab members at the Center for Advanced Diffusion-Wave Technologies (CADIFT) for their friendship and support. Specifically, I would like to acknowledge Dr. Xinxin Guo for her invaluable assistance, lengthy discussions, and suggestions over the years. Thank you to Dr. Alexander Melnikov for his help in the laboratory and Dr. Bahman Lashkari for sharing his knowledge in photoacoustic techniques.

I would also like to recognize Natural Sciences and Engineering Research Council of Canada (NSERC) for financial support of this research project through Engage and Discovery grants and our partner with Alcohol Countermeasure Systems Corp (ACS).

Last but not least, I wish to thank my family for their unconditional love and support in every way possible in all my endeavours.

Table of Contents

Acknowledgments iii

Table of Contents iv

List of Tables vii

List of Figures ix

List of Abbreviations xii

Chapter 1 Introduction 1

1.1 Absorption, Distribution, and Elimination of Alcohol 1

1.2 Behavioural Effects of Alcohol 2

1.3 Drinking and Driving 4

1.4 Research Objective 6

1.5 Organization of Thesis 7

Chapter 2 Alcohol Detection Technology 8

2.1 Tissue Spectrometry 8

2.2 Distant Spectrometry 10

2.3 Electrochemical 12

2.4 Behavioural 13

2.5 Comparison of Alcohol Detection Technologies 15

Chapter 3 WM-DPTR Theory 18

3.1 Photothermal Techniques and Instrumentation and WM-DPTR 18

3.1.1 Excitation Source 18

3.1.2 Modulator 19
3.1.3 Detector 20
3.1.4 Signal Processing 21
3.2 Photothermal Radiometry Signal 21
3.3 WM-DPTR Signal 24
Chapter 4 Research Methodology 29
4.1 Experimental Setup of the WM-DPTR System 29
4.2 Phantoms Preparation 30
4.3 Ethanol Measurement Procedure 32
4.4 Simulations of WM-DPTR System 33
4.5 Calibration Curves and Ethanol Evaluation 36
Chapter 5 Experimental and Simulation Results, Analysis, and Discussion 37
5.1 Characteristics of the WM-DPTR system 37
5.2 Phantom 1 – Water and Ethanol Solutions 39
5.3 Phantom 2 – Blood Serum and Ethanol Solutions 40
5.4 Phantom 3 – Ethanol and Serum Diffused from Skin 42
5.5 Ethanol Measurements with Single-PTR 47
5.6 Experimental and Simulation Results Discussion 49
5.6.1 Comparison between Single-Ended PTR and WM-DPTR Method 49
5.6.2 Dual Channel Measurements and Simulations 49
Chapter 6 Calibration and Evaluation of the Developed Alcohol Biosensor 52
6.1 Ethanol Concentration Estimation from Calibration Curves 52

6.2 Calibration and Evaluation with Common μIR for Amplitude and Phase 53

6.3 Calibration and Evaluation with Different μIR for Amplitude and Phase 56

6.4 Comparison with Other Technologies 59

Chapter 7 Limitations and Future Directions 61

Chapter 8 Significance and Conclusion 63

8.1 Conclusion and Thesis Novel Contributions 63

8.2 Significance 64

References 66

Appendix: Manuscript of First Author Publication 73

List of Tables

Table 1. Effect of Alcohol on Behaviour and Driving [4] 3

Table 2. Comparison of Multiple Alcohol Detection Technologies [30] 16

Table 3. Amount of Pure Ethanol Added to Solution for Obtaining a Given Ethanol Concentration 31

Table 4. Optical and Thermal Property Changes with Varying Ethanol Concentration in Ethanol and Water Solutions 35

Table 5. Optical and Thermal Property Changes with Varying Ethanol Concentration in Ethanol and Serum Solutions 35

Table 6. Optical and Thermal Property Changes with Varying Ethanol Concentration in Human Serum Solutions Diffused through Skin 35

Table 7. WM-DPTR Ethanol Measurement – Phantom 1 39

Table 8. WM-DPTR Ethanol Measurement – Phantom 2 42

Table 9. WM-DPTR Ethanol Measurement – Phantom 3 44

Table 10. WM-DPTR Ethanol Measurement for Quick Roadside Alcohol Tests 46

Table 11. Single-Ended Ethanol Measurement – Phantom 3 47

Table 12. Sensitivity of WM-DPTR-Based Alcohol Biosensor 50

Table 13. Linearity of WM-DPTR-Based Alcohol Biosensor 50

Table 14. Sensitivity and Linearity of Single-Ended PTR Alcohol Biosensor 50

Table 15. Error and Sensitivity of Lock-in Amplifier [47] 51

Table 16. Mean Error and Percent Error between Simulation and Experimental Results 51

Table 17. Ethanol Concentration Estimation Using a Common Fitting Parameter Value for Amplitude and Phase with the System Parameter Combination of R = 0.98, dP = 179.62° .. 56

Table 18. Ethanol Concentration Estimation Using a Common Fitting Parameter Value for Amplitude and Phase with the System Parameter Combination of R = 0.99, dP = 179.68° .. 56

Table 19. Ethanol Concentration Estimation Using Different Fitting Parameter Values for Amplitude and Phase with the System Parameter Combination of R = 0.98, dP = 179.62° .. 59

Table 20. Ethanol Concentration Estimation Using Different Fitting Parameter Values for Amplitude and Phase with the System Parameter Combination of R = 0.99, dP = 179.68° .. 59

Table 21. Comparison with Other Alcohol Detection Technologies – Systematic Error..... 60

Table 22. Comparison with Other Alcohol Biosensors – Standard Deviation 60

List of Figures

Figure 1. Blood Alcohol Concentration over Time after Alcohol Consumption [1] 1

Figure 2. Areas of the Brain Affected by Alcohol [1] 2

Figure 3. MIR Optical Absorption Spectrum of Liquid Ethanol [16] 6

Figure 4. Path of Alcohol in the Body [10] 8

Figure 5. Functional Block Diagram of TruTouch – Tissue Spectrometry [20] 9

Figure 6. Three Layers of Human Skin: Epidermis, Dermis, and Subcutaneous Tissue 10

Figure 7. Autoliv Distant Spectrometry Experimental Setup [22] 11

Figure 8. Electrochemical – Fuel Cell Technology 13

Figure 9. Various Types of Alcohol Detection Technologies (a) TruTouch Prototype (b) Autoliv Prototype (c) ALERT J5 (d) SCRAM Ankle Device [21, 25, 26] 14

Figure 10. Drink Drinking Cues (a) Weaving (b) Stopping Beyond a Limit Line (c) Driving Into Opposing or Crossing Traffic [29] 15

Figure 11. Photothermal Phenomena from Optical Excitation [32] 20

Figure 12. Experimental Setup of Photothermal System with Infrared Detectors [32] 21

Figure 13. PTR Signals from Laser A and Laser B with Transient Delays over 10 Transient Periods 27

Figure 14. Effect of Transient Delay Periods N on PTR Signals from Laser A (a) Q_A (t) and Laser B (b) Q_B (t) 28

Figure 15. WM-DPTR System Configuration 30

Figure 16. Diagram of the Cuvette 32

Figure 17. Amplitude Ratio R Dependence of WM-DPTR Signal at Different Ethanol Concentrations (a) Ethanol-Induced Differential Amplitude Change (b) Ethanol-Induced Differential Phase Change 38

Figure 18. Measured and Simulated WM-DPTR Signals with Ethanol and Water Solutions (a) Differential Amplitude Measurement (b) Differential Phase Measurement 41

Figure 19. Measured and Simulated WM-DPTR Signals with Ethanol and Serum Solutions (a) Differential Amplitude Measurement (b) Differential Phase Measurement 43

Figure 20. Measured and Simulated WM-DPTR Signals with Ethanol and Human Serum Solutions Diffused through Skin (a) Differential Amplitude Measurement (b) Differential Phase Measurement 45

Figure 21. WM-DPTR Phase Ethanol Measurement and Simulation – Quick Roadside Alcohol Tests 47

Figure 22. Single-Ended PTR Measurements with Phantom 3 (a) Single-Ended PTR Amplitude Measurements (b) Single-Ended PTR Phase Measurement 48

Figure 23. Ethanol Calibration Curves Using a Common Fitting Parameter Value for Amplitude and Phase with the System Parameter Combination of R = 0.98, dP = 179.62°: (a) Differential Amplitude and (b) Differential Phase 54

Figure 24. Ethanol Calibration Curves Using a Common Fitting Parameter Value for Amplitude and Phase with the System Parameter Combination of R = 0.99, dP = 179.68°: (a) Differential Amplitude and (b) Differential Phase 55

Figure 25. Ethanol Calibration Curves Using Different Fitting Parameter Values for Amplitude and Phase with the System Parameter Combination of R = 0.98, dP = 179.62°: (a) Differentail Amplitude and (b) Differential Phase 57

Figure 26. Ethanol Calibration Curves Using Different Fitting Parameter Values for Amplitude and Phase with the System Parameter Combination of R = 0.99, dP = 179.68°: (a) Differential Amplitude and (b) Differential Phase 58

Figure 27. New Quantum Cascade Laser Diagram [51] 62

Figure 28. Cell-Phone-Sized Pulsed Diode MIR Lasers Diode [53] 62

List of Abbreviations

ACS	Alcohol Countermeasure Systems
BAC	Blood Alcohol Concentration
BAIID	Breath Alcohol Ignition Interlock Device
BrAC	Breath Alcohol Concentration
DADSS	Driver Alcohol Detection System for Safety
DPTR	Differential PhotoThermal Radiometry
DWI	Driving While Intoxicated
FTIR	Fourier Transform Interferometer
IID	Ignition Interlock Device
IR	Infrared
ISF	Interstitial Fluid
MADD	Mothers Against Drunk Driving
MIR	Mid-InfraRed
MMSE	Minimum Mean Square Error
MSE	Mean Square Error
ND	Neutral Density
NHTSA	National Highway Traffic Safety Administration
NIR	Near InfraRed

PTR	PhotoThermal Radiometry
QCL	Quantum Cascade Laser
SAVE	System for effective Assessment of the driver state and Vehicle control in Emergency situations
SCRAM	Secure Continuous Remote Alcohol Monitoring
SD	Standard Deviation
SE	Systematic Error
SNR	Signal-to-Noise Ratio
WM-DPTR	Wavelength-Modulated Differential PhotoThermal Radiometry

Chapter 1
Introduction

Alcohol has been part of our societies for thousands of years and is used in social, medical, cultural, and religious settings.

1.1 Absorption, Distribution, and Elimination of Alcohol

When an alcohol-containing drink is consumed, the alcohol travels down the throat and esophagus into the stomach. About 20% of the consumed alcohol is diffused into the bloodstream from the stomach while the rest is absorbed in the small intestine. The heart plays the main role in the distribution of alcohol in the body. As the heart pumps the blood, alcohol is transported to the tissues and throughout the water-containing portions of the body. The process of elimination consists of metabolism and excretion. Through the portal vein, the alcohol enters into the liver where alcohol is metabolized. Only about 10% of alcohol that is not metabolized is excreted unchanged through breath, sweat, and urine [1, 2, 3]. The combined effects of absorption, distribution, and elimination produce a characteristic blood alcohol curve as shown in Figure 1[1].

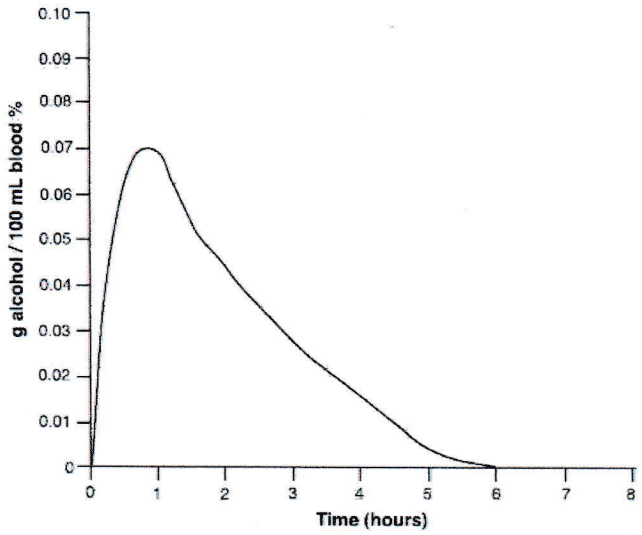


Figure 1. Blood Alcohol Concentration over Time after Alcohol Consumption [1]

Blood alcohol concentration (BAC), defined as grams of ethanol per deciliter of blood, rises sharply during the absorption phase, peaks at 45-90 minutes after consumption, drops quickly during the distribution phase, and declines slowly during the elimination phase [1].

1.2 Behavioural Effects of Alcohol

As mentioned above, during the distribution phase, alcohol is distributed throughout the body, affecting primarily those organs with high water content such as the brain, the "controller" of all human behaviour. So, alcohol consumption induces behavioural changes because alcohol affects various areas of the brain, as shown in Figure 2, including the cerebellum that controls our movement balance, the hippocampus that helps store new memories, the brainstem that controls breathing and circulation, and cerebrum that is responsible for higher brain functions such as sensory perception, reasoning, judgement, emotions, language, and movement [1]. Table 1 shows the effect of alcohol on one's behaviour and driving abilities.

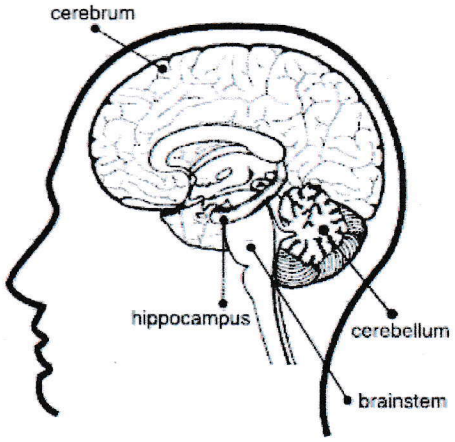


Figure 2. Areas of the Brain Affected by Alcohol [1]

The effect of alcohol on the body and the rate of alcohol absorption and distribution depend on many factors such as food intake and body weight and build. Absorption of alcohol is faster when the stomach is empty during which alcohol passes rapidly into the small intestine where absorption is most efficient. Furthermore, fatty foods require longer digestion time, allowing alcohol absorption to take place over a longer time. Also, those with greater body weight are less

affected by a given amount of alcohol because their body provides a greater volume in which alcohol can be distributed. In addition, since alcohol is more soluble in water than in fat, people with low body fat are less affected by alcohol intake. Since women have smaller body mass and higher proportion of body fat than men, women are more vulnerable to the effects of alcohol and exhibit higher BAC than men after consuming the same amount of alcohol.

Table 1. Effect of Alcohol on Behaviour and Driving [4]

Blood Alcohol Concentration	Typical Effects	Brain Regions Affected	Effects on Driving
0.02 g/dL	- Some loss of judgment - Relaxation	Cerebral cortex	- Declined in visual function - Declined ability to multitask
0.05 g/dL	- Impaired judgment - Lowered alertness - Loss of inhibition	Cerebral cortex	- Reduced coordination and ability to track moving objects - Difficulty in steering - Reduced response to emergency driving situation
0.08 g/dL	- Poor muscle coordination (eg. speech, reaction, vision, hearing, and balance) - Impaired judgment, self-control, reasoning, and memory	Cerebral cortex and forebrain	- Loss of concentration and short-term memory - Reduced speed control and information processing capability - Impaired perception
0.10 g/dL	- Slurred speech, poor coordination, and slowed thinking	Cerebral cortex and forebrain	- Reduced ability to maintain lane position and brake appropriately
0.15 g/dL	- Vomit may occur - Major loss of balance	Cerebral cortex, forebrain, and cerebellum	- Substantial impairment in vehicle control, attention to driving task, and visual and auditory information processing

As a rule of thumb, to stay under 0.05 g/dL:

- Men can drink two standard drinks in the first hour and one additional drink each additional hour.
- Women can drink one standard drink in the first hour and one additional drink each additional hour.

One standard drink contains 13.5 grams of ethanol. 341 ml (12 oz.) bottle of beer, 148 ml (5 oz.) glass of wine, and 44 ml (1.5 oz.) shot of spirits are each considered one standard drink [1]. Ethanol is the alcohol contained in alcoholic beverages and the two terms, alcohol and ethanol, are used interchangeably throughout this thesis.

1.3 Drinking and Driving

In Canada, alcohol-impaired driving is the leading cause of criminal deaths [5]. It is estimated that 32% of all automobile crash deaths are a direct result of drunk driving and one in every three people will be involved in an alcohol related vehicle crash in their lifetime [6]. Although we spared no effort in reducing the number of drinking and driving incidents, the number of impaired driving incidents is still on the rise [7]. For example, police in 2011 reported 90 277 impaired driving incidents in which the drivers' BAC was over the legal limit of 0.08 g/dL. This is about 3,000 more incidents than in 2010 [5, 8].

Many countermeasures such as fines, incarceration, vehicle impoundment, and license revocation are used to prevent drunk driving. However, these tactics are not very effective. Incarceration is costly while the effects of vehicle impoundment are not limited to the drunk driver. License revocation has its limitations as studies have shown that up to 75% of drivers with suspended licenses continue to drive illegally and violators who receive fines do not modify their driving habits [9].

Some provinces in Canada have their own policy to reduce drunk driving. For example, in Ontario, an ignition interlock device (IID) may be installed in the vehicles of those convicted of driving while intoxicated (DWI) [10]. Although studies indicate that IIDs can reduce recidivism by about two-thirds, the probability of arrest while driving with a blood alcohol level over the legal limit is about one in 200 [9, 11]. To overcome this drawback, Mothers Against Drunk Driving (MADD) has called for ignition interlocks to become standard equipment in all motor vehicles sold [12]. Meanwhile, Driver Alcohol Detection System for Safety (DADSS) has suggested that in-vehicle alcohol detection technologies suitable for use in all-vehicle should be

non-invasive, reliable, durable, quick to use, and seamless with the driving task and require little or no maintenance [13].

Most of today's IIDs are breath ignition interlock devices (BAIIDs) consisting of a handheld sensor-and-display unit with an under-dash unit that interfaces to the vehicle's ignition and power circuits. The controller first turns on the heater in the fuel cell. Once the operating temperature is reached, the driver is asked to take a deep breath and blow long and hard. The pressure and air flow sensors determine if the breath sample is acceptable. If the blown sample is acceptable and the measured breath alcohol concentration (BrAC) is less than the programmed alcohol limit, the driver can start the vehicle normally. If the measured BrAC exceeds the limit, the ignition is locked out for some period of time and the controller signals for another sample after some period of time, typically 5 to 30 minutes. During driving, the driver is asked to provide breath sample at random intervals. In such cases, drivers need to pull over out of traffic to perform the retest.

Compared to DADSS' suggested specifications for alcohol detection technologies, current BAIIDs have limitations. They are sensitive to changes in the environment. In fact, one analyst who examined large numbers of BAIID data records notes, in numerous cases, substantial differences in breath alcohol concentration readings taken only a few minutes apart. Since BAIIDs use fuel-cell sensors that must be warmed up to breath temperature to meet the accuracy specification, they use significant energy for heating and take longer than 30 seconds for measurement. Also, current fuel-cell sensors exhibit some drift in response, about 1 percent of the reading per month, requiring very frequent maintenance and calibration services. In addition, they require the driver to deliver a delicate breath into the device before starting a vehicle and in random running retests during driving, distracting the driver from the driving task. Serious accidents have occurred due to distraction associated with retests [14]. Consequently, developing a new in-vehicle BAC biosensor is the key to improving ignition interlocks.

1.4 Research Objective

In this research, the main objective is to develop an ethyl alcohol biosensor using Wavelength-Modulated Differential Photothermal Radiometry (WM-DPTR) technology.

WM-DPTR is a non-invasive method used to measure minute absorption of low-concentration solutes in strongly absorbing fluids like water and blood by suppressing the strong background signal due to water absorption and other baseline variations through differential measurements at the peak (~ 9.5 μm or 1042 cm^{-1}) and the baseline (~ 10.4 μm or 962 cm^{-1}) of the ethanol absorption band, as shown in Figure 3, and eliminating source-detector interference using the lock-in amplifier to enhance alcohol detection selectivity, accuracy, and precision [15].

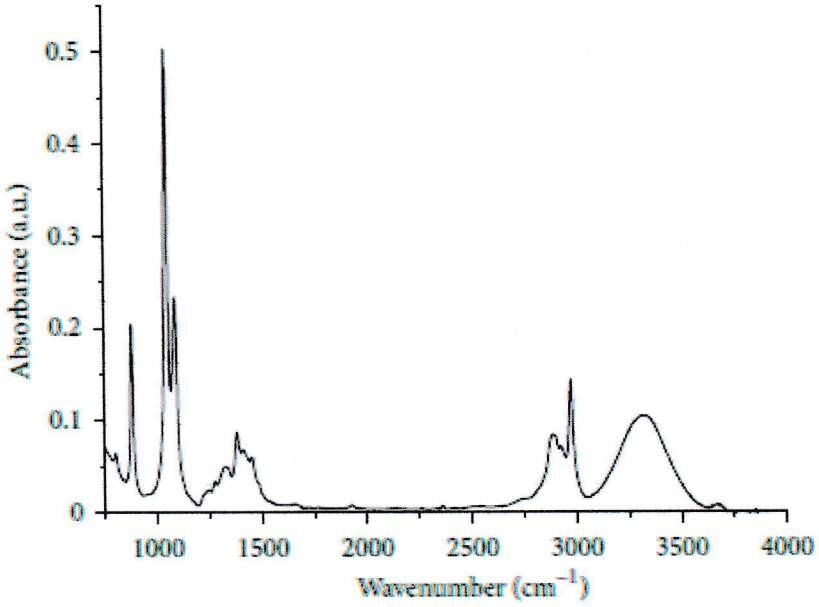


Figure 3. MIR Optical Absorption Spectrum of Liquid Ethanol [16]

The advantages of the WM-DPTR method can be highlighted from its photothermal and sensitivity tunability properties. The photothermal property of WM-DPTR greatly enhances signals strength as the thermal effusivity change acts as an amplifying factor of the optical absorption coefficient change [17]. This allows the WM-DPTR system to overcome the difficulty associated with the MIR shallow optical penetration from strong optical scattering and enables

the system to measure BAC as mirrored in the interstitial fluid (ISF) in dermis [15, 18]. By making good use of its sensitivity tunability property and carefully selecting the system parameters, namely intensity ratio and phase difference combination of laser beams, the system can be optimized for high BAC measurement accuracy, precision, and sensitivity [19].

1.5 Organization of Thesis

The remaining sections are divided as follows. Chapter 2 gives a literature review of current alcohol technologies while Chapter 3 describes the principles and theory of WM-DPTR. Chapter 4 focuses on research methodology including experimental setup, the process of making phantoms, ethanol measurement procedure, the development of the WM-DPTR simulator, and the biosensor calibration method. The experimental and simulations results are shown, analyzed, and discussed in Chapter 5. In addition, in Chapter 6, the developed alcohol biosensor is calibrated using calibration curves using which the developed biosensor is evaluated in terms of sensitivity, linearity, accuracy, precision, and measurement time and compared with other alcohol biosensors on the market and under development. The limitation of the work and potential future directions are mentioned in Chapter 7. A summary of the work, its contributions, and its significance are found in Chapter 8.

Chapter 2
Alcohol Detection Technology

Due to the limitations of current BAIIDs, multiple new alcohol detection technologies are under development. As illustrated in Figure 4, most alcohol detection technologies determine BAC from the person's skin, sweat, breath, and behaviour since measuring BAC from the urine is not feasible and measuring BAC from the blood is too invasive.

As a result, current and new technologies for alcohol detection can be grouped into one of four technology types: tissue spectrometry, distant spectrometry, electrochemical, and behavioural systems.

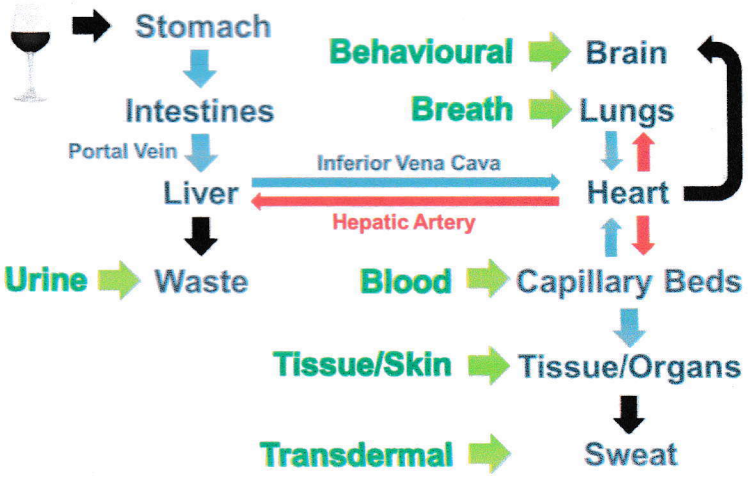


Figure 4. Path of Alcohol in the Body [10]

2.1 Tissue Spectrometry

Tissue spectrometry systems determine BAC non-invasively from the alcohol content of the ISF in the dermis by measuring how much light has been absorbed at a particular wavelength from a near-infrared (NIR) beam reflected from the subject skin. Since light absorption occurs at

resonance wavelengths, this technology makes use of numerous resonances of ethanol molecules in the NIR spectrum.

The invention of this technology led to the development of TruTouch, a new alcohol detection device that employs NIR absorption spectroscopy from 1.25 to 2.5 μm to interrogate the alcohol concentration in the epidermal layer of skin tissue. Figure 5 depicts the functional block diagram of TruTouch.

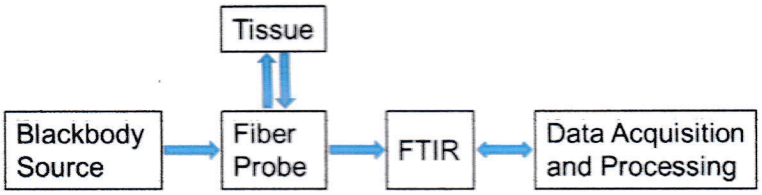


Figure 5. Functional Block Diagram of TruTouch – Tissue Spectrometry [20]

NIR light is generated using a ceramic blackbody source operating at 1100°C. A fibre optic probe delivers the light into the user's skin and collects the backscattered light which is collimated and coupled into a Michelson Fourier Transform Interferometer (FTIR) with an optical resolution of 32 cm^{-1}. The optical interferogram signal is collected using an InGaAs photodiode and digitized using an analog to digital converter. The signal is then transformed, using standard FTIR data processing techniques, to absorbance spectra that is finally converted into blood alcohol concentration measurements via a fixed partial least squares calibration model. An embedded computer controls the FTIR, performs data acquisition and data processing, and serves as the user interface. The measurement process takes about 30 seconds.

During BAC measurement, the fibre optic probe is designed to interrogate to the dermal layer of skin since, out of the three main layers of the skin, namely epidermal, dermal, and subcutaneous layers, as illustrated in Figure 6, the dermal layer is the best layer of skin tissue for alcohol measurements. Unlike the epidermis that contains very little extracellular fluid and the subcutaneous layer that is largely comprised of lipids which are hydrophobic, the dermal layer

has high water content and an extensive capillary bed conducive to the transport of alcohol, a hydrophilic analyte [20].

However, TruTouch's selectivity is limited by weak ethanol absorption in NIR and confounding absorptions from other skin tissue components, such as skin pigments, to which NIR tissue spectroscopy is sensitive. In addition, the measurement accuracy is affected by various characteristics of the detector such as bandwidth, noise, linearity, and stability. In general, alcohol detection based on tissue spectrometry takes too much time to perform ethanol measurement to be viable for use in interlocks. TruTouch can achieve accuracy of 0.0001 g/dL with standard deviation of 0.0016 g/dL at an ethanol concentration of 0.080 g/dL. A prototype of TruTouch is shown in Figure 9a.

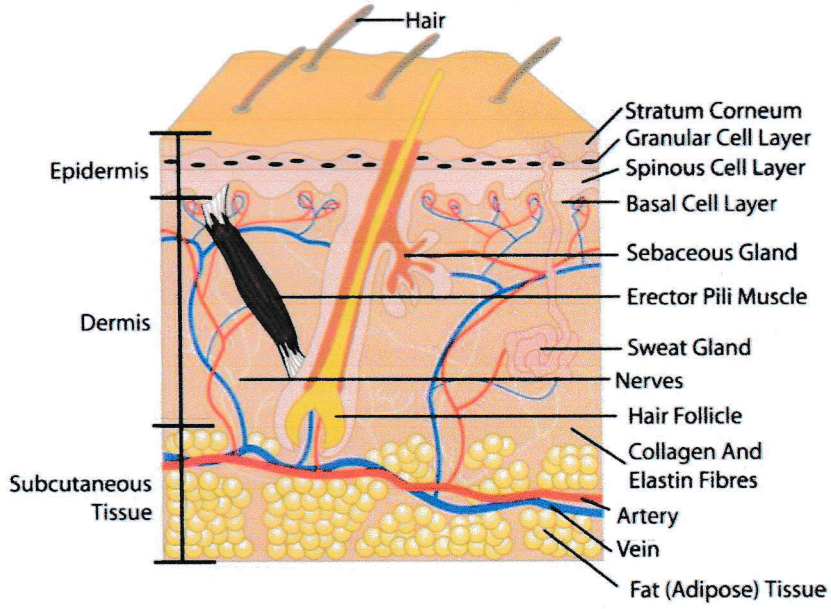


Figure 6. Three Layers of Human Skin: Epidermis, Dermis, and Subcutaneous Tissue
Taken from http://www.seabuckthorn.com/images/Skindiagam.jpg

2.2 Distant Spectrometry

Alcohol detection technologies based on distant spectrometry aim to remotely analyze BAC by using measurements of exhaled carbon dioxide CO_2 based on mid-infrared spectroscopy as an

indication of the degree of dilution of the alcohol in exhaled air [21]. The breath alcohol concentration C_{BrAC} can be assessed from external measurements of alcohol $C_{extEtOH}$ and CO_2 C_{extCO2} using Equation 1.

$$C_{BrAC} = \frac{C_{extEtOH}}{C_{extCO2}} C_{alvCO2} \quad (1)$$

Here, the assumption is that the alveolar CO_2 concentration C_{alvCO2} is known or predictable, whereas its concentration in ambient air is close to zero. Generally, C_{alvCO2} is normally, in terms of partial pressure, 5.3 kPa or 40 mm Hg and is higher with physical activity and lung dysfunctions.

The Autoliv system works based on the principles of distant spectrometry and determines BrAC using infrared spectroscopy based on light absorption due to molecular vibration of ethanol at its fundamental absorption band of 9.5 µm or 1042 cm^{-1}. Figure 7 shows the experimental setup which includes one commercial catalytic alcohol sensor and one electroacoustic CO_2 sensor, both mounted inside a small piece of Perspex tubing. Analog output signals from each of the sensors are digitized and processed using standard equipment from National Instruments [22].

During measurement, the cabin air is drawn into the car into the optical module through the breathing cup, as depicted in Figure 9b, and is analyzed by the detector to determine the external concentration of ethanol and CO_2. The entire process takes about 5 seconds.

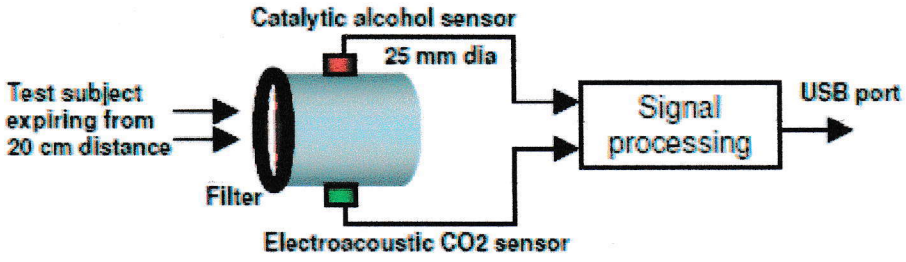


Figure 7. Autoliv Distant Spectrometry Experimental Setup [22]

Since multiple sensors need to be placed strategically around the cabin of the vehicle close to the driver to determine BrAC, one challenge in distant-spectrometry-based BAC biosensors is to determine the number and placement of sensors which enables BrAC to be measured quickly and accurately given the dynamics of the cabin air because the direction of the expired airflow affects the signal quality [21]. In addition, alveolar CO_2 concentration varies from person to person and with physical activity and lung functions. This complicates the calibration procedure and introduces false readings [19]. The Autoliv system can achieve accuracy of 0.0008 g/dL with standard deviation of 0.0022 g/dL at an ethanol concentration of 0.080 g/dL. [21].

2.3 Electrochemical

One type of electrochemical sensor works by measuring colorimetric changes produced by alcohol in the presence of reactant chemicals as described in the following chemical equation, catalyzed by silver nitrate $AgNO_3$:

$$2\ K_2Cr_2O_7 + 3\ CH_3CH_2OH + 8\ H_2SO_4 \rightarrow 2\ Cr_2(SO_4)_3 + 2\ K_2SO_4 + 3\ CH_3COOH + 11H_2O$$

During the redox reaction, the reddish-orange dichromate ion $Cr_2O_7^-$ changes to green chromium ion Cr^{3+}. These sensors consist of two glass vials, each containing the same amount of reactants, and a photocell system, hooked to a meter for measuring the color change due to the chemical reaction. The breath sample is bubbled through one vial. The reacted mixture in the first vial is compared, using the photocell system, to the other vial containing the un-reacted mixture to determine BrAC.

The gold standard technology for electrochemical sensor is fuel cell technology, as illustrated in Figure 8 [23]. During the fuel cell reaction, the platinum oxidizes any alcohol content in the air and produces acid, protons and electrons. The process can be characterized by the following redox reaction:

$$C_2H_5OH + H_2O \rightarrow CH_3COOH + 4H^+ + 4e^-$$
$$O_2 + 4H^+ + 4e^- \rightarrow 2H_2O$$

The greater level of alcohol in the air is oxidized, the more electrons produced by the reaction, resulting in a greater output current which is used to determine BAC [24].

Electrochemical sensors come in two types: breathalyzers and transdermal sensors. Breathalyzer sensors estimate BAC from breath samples [25]. Alcohol Countermeasure Systems' (ACS) ALERTJ5, as shown in Figure 9c, is an example of such device. It can achieve an accuracy of ±0.005 g/dL at 0.100 g/dL [26].

Transdermal or sweat sensors are body-worn perspiration monitors. These are not as accurate as fuel-cell-based BrAC sensor since alcohol takes from 30 minutes to two hours to appear in perspiration. One transdermal-based alcohol sensor is the Secure Continuous Remote Alcohol Monitoring (SCRAM) device shown in Figure 9d. SCRAM is worn around the ankle and prescribed by many U.S. courts for serious alcohol offenders [25]. According to a report by National Highway Traffic Safety Administration (NHTSA), the device can only correctly detect BAC equal to or higher than 0.02 g/dL in 155 of the 271 tests or in 57.2% of the tests [27].

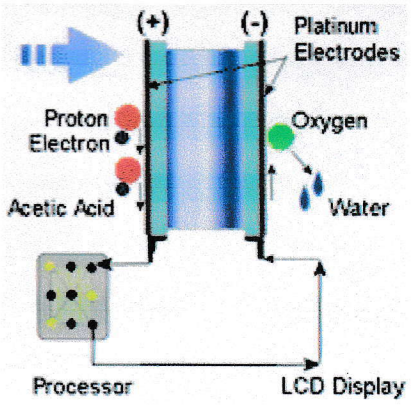


Figure 8. Electrochemical – Fuel Cell Technology
[Taken from https://www.breathalyzercanada.com]

2.4 Behavioural

Recently, behavioural-based alcohol detection technologies emerge as new potential technologies. These systems attempt to identify cues of typical drunk driving behaviour. In the

drunk driving detection system developed by Dai et al., the cues can be categorized into three categories: (1) cues related to lane position maintenance problems such as weaving, drifting, swerving, and turning abruptly or with a wide radius; (2) cues related to speed control problems such as accelerating or decelerating suddenly or stopping beyond a limit line; and, (3) cues related to judgment and vigilance problems such as driving with tires on lane marker, driving on the other side of the road or into opposing traffic, and slow response to traffic signals. Some of the above cues are illustrated in Figure 10. However, the specificity of such system is low because, if one of the behavioural cues is observed, one can only conclude that the driver can be drunk driving. For example, if a driver is observed to be weaving, he is about 50% likely to be drunk driving [28].



(a) (b)

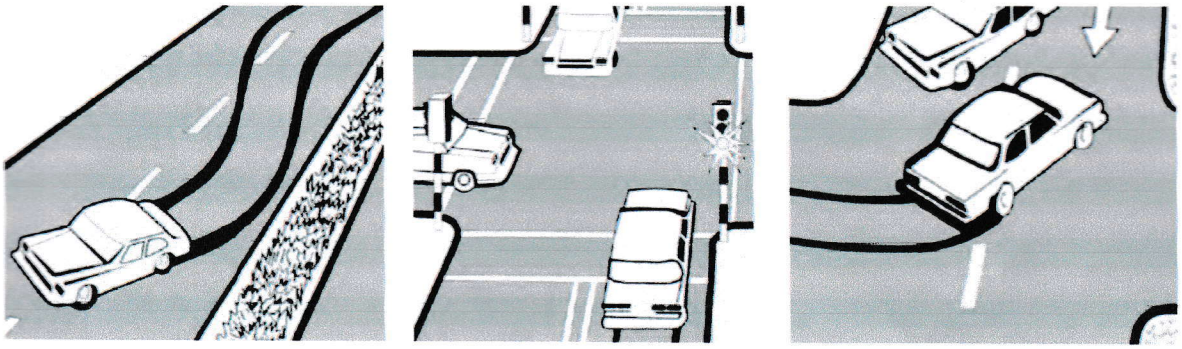
(c) (d)

Figure 9. Various Types of Alcohol Detection Technologies (a) TruTouch Prototype (b) Autoliv Prototype (c) ALERT J5 (d) SCRAM Ankle Device [21, 25, 26]

In project SAVE (System for effective Assessment of the driver state and Vehicle control in Emergency situations), to determine whether or not the driver is driving with BAC of equal or

greater than 0.05 g/dL, different neural-network-based machine learning algorithms are fed with data from multiple sensors that look for the following behavioural cues [29]:

- Eye blink,
- Eyelid closure,
- Steering wheel grip,
- Mean lane position (relative to right lane marking),
- Standard deviation of lane position,
- Standard deviation of steering wheel position,
- Mean speed,
- Standard deviation of speed, and
- Time to lane crossing.



(a) (b) (c)

Figure 10. Drink Drinking Cues (a) Weaving (b) Stopping Beyond a Limit Line (c) Driving Into Opposing or Crossing Traffic [29]

Their false-alarm rate for the behavioural system is orders of magnitude higher than that of current breath-alcohol ignition interlocks. The accuracy is much higher if personalized baselines were used which would mean that the "natural" behaviour of the driver must be known before predicting whether the driver is impaired or not.

2.5 Comparison of Alcohol Detection Technologies

The four types of technologies described in this chapter can be ranked in terms of [30]:

- Accuracy
- Cost – unit cost for fully developed technology in mass production
- Development time – years to reach mass production of units and be used widely
- Convenience – usability of the device
- Circumvention risk – vulnerability of sensor to being fooled into providing a low estimate of BAC
- Technical risk – risk that the technology will never reach the mass-market

Table 2 summaries the rankings.

Table 2. Comparison of Multiple Alcohol Detection Technologies [30]

Technologies	**Criteria**					
	Accuracy	Cost	Development Time	Convenience	Circumvention Risk	Technical Risk
Tissue Spectrometry	+++	?	-	+++	++	--
Distant Spectrometry	--	++	+	+++	---	+++
Electro-chemical	+	+	++	-	+++	++
Behavioural	-	++	-	+++	--	---

Scale: Best +++ to Worst ---

One of the main advantages of tissue spectroscopy is its accuracy which relies on complex regression analysis and statistical processes of the reflectance spectrum from the subject's skin. Also, it avoids the sensor contamination and reduces measurement-drift problems. Another advantage is usability because it requires minimal end-user effort to measure ethanol concentration. Since the diffusion time from blood to tissue is about 15 minutes, drunk driving can be quickly detected. However, tissue spectroscopy is still in an early stage of development.

Like tissue spectrometry, distant-spectrometry-based technologies are very user friendly in that minimal user interaction is required. However, it could take some time for the system to determine if impairment exists.

The electrochemical biosensors using fuel-cell sensors have been used in ignition interlocks for years and are continuously improved. This technology is fairly robust, ethanol-specific, and accurate if the fuel cell is warmed up to breath temperature before ethanol measurement. With routine servicing and recalibration, data downloading, and reporting, those alcohol sensors cost about $900 per year per vehicle. One main disadvantage of such technology is that it demands user participation – the user has to blow in a strong long breath and pull over for retests on the roads.

Transdermal sensors are relatively cheap. According to the manufacturer, the daily cost of the SCRAM system is $10 to $12 per day. It can take a long time to detect impairment due to the influence of alcohol because of the long latency for alcohol to appear in perspiration. However, the accuracy of the sensors is affected by differences between people in sweating rate, skin thickness and permeability. In addition, although they avoid the inconvenience of performing the breath test because they are worn continuously, contamination of biosensor is a substantial problem, wearing it can be uncomfortable, and some users find it embarrassing to wear them.

Similar to distant-spectrometry, behavioural-based impairment monitors require no user participation. However, the installation of such system costs several thousand dollars due to expensive sensors and processors. In most cases, impairment can be detected within a minute. However, in the absence of traffic or driving obstacles, detection may be much delayed or never occur at all.

Chapter 3
WM-DPTR Theory

In this thesis, a new type of alcohol detection technology is developed using WM-DPTR method. The method is based on photothermal science. This chapter gives a summary of the model for WM-DPTR signals as well as a review of basic photothermal techniques and instrumentation. The detailed theoretical derivation of mathematical model for WM-DPTR signals is given in [31].

3.1 Photothermal Techniques and Instrumentation and WM-DPTR

Photothermal science encompasses a variety of techniques and phenomena involving the conversion of absorbed optical energy into thermal energy or heat. During this process, the excited electronics states, resulted from the selective absorption processes, in the atoms or molecules lose their energy by a series of non-radioactive transitions that result in heating of the material.

The main components of a photothermal system are:

- Excitation source
- Modulator
- Detector
- Signal processing and display system

3.1.1 Excitation Source

The light source generated modulated heating in a sample medium. Photothermal sources fall into two categories:

- Incoherent sources for spectroscopic applications
- Coherent sources or lasers

In the WM-DPTR system, lasers are used as excitation sources.

3.1.2 Modulator

Many methods have been used to modulate the source or, in other words, impose a temporal variation on the optical energy applied to the sample and they include:

- Periodic (ie. Sinusoidal or square waves)
- Transient
- Frequency multiplexed (ex. Frequency-modulated)
- Spatially modulated

In this research, the laser is modulated by a square wave through direct electrical modulation where the optical output changes by varying the electrical current. The modulating frequency impacts the probing depth in that the thermal diffusion length μ is:

$$\mu = \sqrt{\frac{\alpha}{\pi f}}$$

where α is the thermal diffusivity and f the modulation frequency. The above equation implies that a highly diffusive material or low modulation frequency enhances the propagation and detection of thermal waves deeper into the medium. In WM-DPTR system, the modulation frequency is set at 90 Hz to probe in the dermis layer of the skin.

The modulated heating results in a number of physical changes in and around the sample, as illustrated in Figure 11, including:

- Temperature increase
- Infrared emission
- Surface distortion due to thermal expansion
- Acoustic wave generation and propagation
- Thermal refractive index gradient

3.1.3 Detector

Based on the heating effects of the sample, three detection schemes are used for the detection of resultant thermal waves:

- Acoustic methods, in which either a gas condenser microphone is used for the detection of pressure variations in air or a piezoelectric transducer for the detection of thermo-elastic waves in solid media
- Optical methods, in which probe beams and photo-detectors are employed to monitor variations in the optical properties of a heated sample or the medium surrounding the sample
- Thermal methods, in which thermocouples, thermistors, infrared detectors or pyro-electric transducers are used to detect thermal waves directly

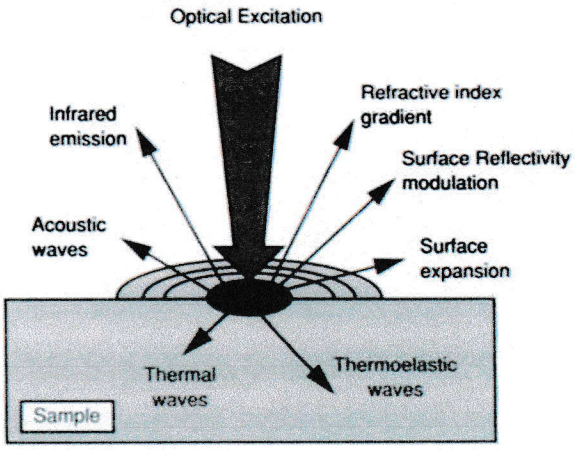


Figure 11. Photothermal Phenomena from Optical Excitation [32]

In this research, infrared detectors are used to detect thermal waves because the method of infrared detection is simple, robust, non-contacting, and compatible with many industrial requirements. The effectiveness of infrared detection depends on maximizing the infrared radiation collected by the detector and minimizing the incidence of the excitation source radiation on the detector. The former is achieved by using suitable infrared collecting optics such as lenses and parabolic mirrors and placing the detector close to the sample while the latter is fulfilled by the use of filers and the geometry arrangement of the system to prevent the detector

from being exposed to source radiation. Figure 12 describes the use of infrared detectors in a photothermal experimental setup [32].

3.1.4 Signal Processing

In terms of signal processing, the WM-DPTR method employs a lock-in amplifier so that the generated amplitude and phase signals can achieve improved Signal-to-Noise Ratio (SNR) compared to time-domain methods [33].

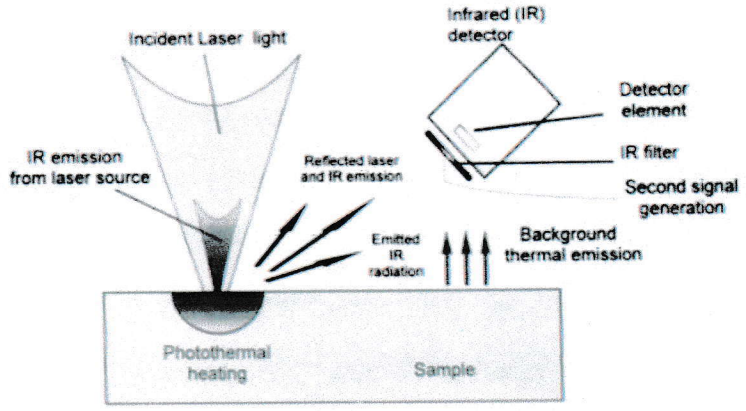


Figure 12. Experimental Setup of Photothermal System with Infrared Detectors [32]

3.2 Photothermal Radiometry Signal

WM-DPTR is based on photothermal radiometry (PTR) principle. When light is absorbed by a sample, a semi-infinite one-dimensional medium, the transient temperature field of the sample is

$$T_m(z,t) = T_o + \Delta T_m(z,t) \quad (2)$$

where T_o is the thermal equilibrium temperature and $T_m(z,t)$ is the temperature increase in the sample. The resulting infrared (IR) radiation intensity is described by the Planck distribution function:

$$W_p(z,\lambda,T_m) = W_p(z,T_o) + \Delta W_p[\lambda,T_m(z,t)] \quad (3)$$

where

$W_p(\lambda, T_o) = \frac{2\pi hc^2}{\lambda^5\left[\exp\left(\frac{hc}{\lambda k_B T_o}\right)-1\right]}$ is the Planck distribution function describing the blackbody spectral radiant emittance at IR wavelength λ at thermal equilibrium,

$\Delta W_p[\lambda, T_m(z,t)] = \frac{W_p(\lambda,T_o)\left(\frac{hc}{\lambda k_B T_o}\right)}{\left[\exp\left(\frac{hc}{\lambda k_B T_o}\right)-1\right]}\left[\frac{\Delta T_m(z,t)}{T_o}\right]$ is the IR radiation increase due to increase in temperature,

h is Planck's constant,

c is the speed of light in vacuum, and

k_B is the Boltzmann constant.

The IR thermophotonic emissive signal increases upon turning the laser beam on is:

$$\Delta Q(t) = K(\lambda_1, \lambda_2)\bar{\mu}_{IR}\int_0^\infty e^{-\bar{\mu}_{IR}z}\,\Delta T_m(z,t)\,dz \qquad (4)$$

where

$\bar{\mu}_{IR} = \frac{\int_{\lambda_1}^{\lambda_2} W_p(\lambda,T_o)\,\mu_{IR}(\lambda)\,d\lambda}{\int_{\lambda_1}^{\lambda_2} W_p(\lambda,T_o)\,d\lambda}$ is the spectrally weighted IR emission coefficient for the sample,

$K(\lambda_1, \lambda_2) = \frac{hc}{k_B T_o^2}\frac{\int_{\lambda_1}^{\lambda_2} W_p(\lambda,T_o)\,d\lambda}{\lambda\left[\exp\left(\frac{hc}{\lambda k_B T_o}\right)-1\right]}$ is a factor related to the IR detector bandwidth $[\lambda_1, \lambda_2]$, and $\mu_{IR}(\lambda)$ is the IR absorption (emission) coefficient of the sample at wavelength λ. In practice, $\bar{\mu}_{IR}$ is a fitting parameter to experimental data.

The photothermal impulse response to an instantaneous optical pulse of Dirac $\delta(t)$ and intensity I_o, which generates a thermal power density depth profile of $F(z,t) = I_o\mu_e e^{-\mu_e z}\,\delta(t)$ with $0 \le z < \infty$ and is subjected to the adiabatic boundary condition $\left.\frac{\partial T(z,t)}{\partial z}\right|_{z=0} = 0$ at the sample-air interface, is found using Green function method to be

$$T_m(z,t) = \frac{I_o \alpha \mu_e}{2k} \left\{ e^{-\mu_e z} erfc\left(\sqrt{\frac{t}{\tau_t}} - \frac{z}{2\sqrt{\alpha t}} \right) + e^{\mu_e z} erfc\left(\sqrt{\frac{t}{\tau_t}} + \frac{z}{2\sqrt{\alpha t}} \right) \right\} e^{\frac{t}{\tau_t}} \quad (5)$$

where α is the thermal diffusivity,

μ_e is the absorption coefficient,

k is the thermal conductivity of the sample,

$\tau_t \equiv \frac{1}{\mu_e^2 \alpha}$ is a photothermal time constant, and

$erfc\,(y) = \frac{2}{\sqrt{\pi}} \int_0^\infty e^{-x^2} dx.$

For a rectangular finite optical pulse

$$I(t) = I_o \begin{cases} 1; & 0 \le t \le \tau_p \\ 0; & \tau_p \le t \le \tau_o \end{cases} \quad (6)$$

where τ_p is the pulse duration and τ_o is the pulse repetition period. The temperature transient can be expressed as a convolution integral of the photothermal impulse response.

For $0 \le t \le \tau_p$, one can show, using Equation 5:

$$\begin{aligned} \Delta T_{m1}(z,t) &= I_o \int_0^t \Delta T_m(z, t-\tau)\, d\tau \\ &= \frac{I_o \alpha \mu_e}{2k} \left\{ \begin{aligned} & e^{-\mu_e z} e^{\frac{t}{\tau_t}} \int_0^t e^{-\frac{\tau}{\tau_t}} erfc\left(\sqrt{\frac{t-\tau}{\tau_t}} - \frac{z}{2\sqrt{\alpha(t-\tau)}} \right) d\tau \\ & + e^{\mu_e z} e^{\frac{t}{\tau_t}} \int_0^t e^{-\frac{\tau}{\tau_t}} erfc\left(\sqrt{\frac{t-\tau}{\tau_t}} + \frac{z}{2\sqrt{\alpha(t-\tau)}} \right) d\tau \end{aligned} \right\} \end{aligned} \quad (7)$$

For $\tau_p \le t \le \tau_o$, one can show, using Equations 5 and 7:

$$\Delta T_{m2}(z,t) = I_o \int_0^{\tau_p} \Delta T_m(z, t-\tau)\, d\tau \tag{8}$$

$$= \frac{I_o \alpha \mu_e}{2k} \left\{ \begin{array}{l} e^{-\mu_e z} e^{\frac{t}{\tau_t}} \int_0^{\tau_p} e^{-\frac{\tau}{\tau_t}} erfc\left(\sqrt{\frac{t-\tau}{\tau_t}} - \frac{z}{2\sqrt{\alpha(t-\tau)}} \right) d\tau \\ + e^{\mu_e z} e^{\frac{t}{\tau_t}} \int_0^{\tau_p} e^{-\frac{\tau}{\tau_t}} erfc\left(\sqrt{\frac{t-\tau}{\tau_t}} + \frac{z}{2\sqrt{\alpha(t-\tau)}} \right) d\tau \end{array} \right\}$$

$$= \Delta T_{m1}(z,t) - \Delta T_{m1}(z, t-\tau_p)$$

From Equations 4 and 7, the PTR response to a rectangular optical pulse described above is

$$\Delta Q(t) = \frac{I_o \alpha \mu_e \bar{\mu}_{IR}}{2k} K(\lambda_1, \lambda_2)\, \tau_t \left\{ \begin{array}{l} \frac{1}{\bar{\mu}_{IR} + \mu_e} \left[W\left(\sqrt{\frac{t}{\tau_t}} \right) + W\left(\sqrt{\frac{t}{\tau_{IR}}} \right) - 2 \right] \\ + \frac{1}{\bar{\mu}_{IR} - \mu_e} \left[W\left(\sqrt{\frac{t}{\tau_t}} \right) - W\left(\sqrt{\frac{t}{\tau_{IR}}} \right) \right] \\ + \frac{2}{\bar{\mu}_{IR}} \left\{ 2\sqrt{\frac{t}{\pi \tau_t}} - \sqrt{\frac{\tau_{IR}}{\tau_t}} \left[1 - W\left(\sqrt{\frac{t}{\tau_{IR}}} \right) \right] \right\} \end{array} \right\} \tag{9}$$

where $W(x) = e^{x^2} erfc(x)$ and $\tau_{IR} \equiv \frac{1}{\bar{\mu}_{IR}^2 \alpha}$ is another photothermal time constant. The PTR response for $\tau_p \le t \le \tau_o$ is thus $\Delta Q(\tau_p \le t \le \tau_o) = \Delta Q(t) - \Delta Q(t - \tau_p)$.

3.3 WM-DPTR Signal

For the WM-DPTR system with lock-in detection, only laser A is turned on during $0 \le t \le \tau_p$ and generates DPTR response ΔQ_A while only laser B is turned on during $\tau_p \le t \le \tau_o$ and generates DPTR response ΔQ_B with τ_o set to the repetition period of the modulated pulse and $\tau_p = \frac{\tau_o}{2}$. Equation 9 can be generalized to

$$\Delta Q_j(t) = \frac{I_o \alpha \mu_{ej}\, \bar{\mu}_{IR}}{2k} K(\lambda_1, \lambda_2)\, \tau_{tj} \left\{ \begin{array}{l} \dfrac{1}{\bar{\mu}_{IR} + \mu_{ej}} \left[W\left(\sqrt{\dfrac{t}{\tau_{tj}}}\right) + W\left(\sqrt{\dfrac{t}{\tau_{IR}}}\right) - 2 \right] \\ + \dfrac{1}{\bar{\mu}_{IR} - \mu_{ej}} \left[W\left(\sqrt{\dfrac{t}{\tau_{tj}}}\right) - W\left(\sqrt{\dfrac{t}{\tau_{IR}}}\right) \right] \\ + \dfrac{2}{\bar{\mu}_{IR}} \left\{ 2\sqrt{\dfrac{t}{\pi \tau_{tj}}} - \sqrt{\dfrac{\tau_{IR}}{\tau_{tj}}} \left[1 - W\left(\sqrt{\dfrac{t}{\tau_{IR}}}\right) \right] \right\} \end{array} \right\}; \; j = A, B \tag{10}$$

For the full period $0 \le t \le \tau_o$, the DPTR response can be described as:

$$S_{AB}(t) = \begin{cases} \Delta Q_A(t) & 0 \le t \le \tau_p \\ \Delta Q_A(t) - \Delta Q_A(t - \tau_p) + \Delta Q_B(t - \tau_p) & \tau_p \le t \le \tau_o \end{cases} \tag{11}$$

To take into account the decaying transient from laser B during the period $-\tau_o \le t \le 0$, Equation (11) can be refined to:

$$S_{AB}(t) = \begin{cases} \Delta Q_A(t)\, u(t) - \Delta Q_A(t - \tau_p) u(t - \tau_p) \\ + \Delta Q_B(t - \tau_p) u(t - \tau_p) + \Delta Q_B(t + \tau_p) - \Delta Q_B(t) \end{cases}; \; 0 \le t \le \tau_o \tag{12}$$

where u (t) is the unit step or Heaviside function.

In most cases, the transient decays are slow and occur over N periods as illustrated in Figure 13 for N=10. Thus, S_{AB} should include contributions from earlier decaying transients from lasers A and B from prior N periods. The complete set of signal contributions from photothermal transients of earlier periods is:

$$S_{AB0}(t) = \begin{cases} \Delta Q_A(t)\, u(t) - \Delta Q_A(t - \tau_p) u(t - \tau_p) \\ + \Delta Q_B(t - \tau_p) u(t - \tau_p) \end{cases}; \; 0 \le t \le \tau_o$$

$$S_{AB-1}(t) = \begin{cases} \Delta Q_A(t + \tau_0)\, u(t + \tau_0) - \Delta Q_A(t + \tau_p) u(t + \tau_p) \\ + \Delta Q_B(t + \tau_p) u(t + \tau_p) - \Delta Q_B(t) u(t) \end{cases}; \; -\tau_o \le t \le 0 \tag{13}$$

$$\vdots$$

$$S_{AB-N}(t) =$$

$$\begin{cases} \Delta Q_A(t+N\tau_0)\,u(t+N\tau_0) - \Delta Q_A(t+N\tau_0-\tau_p)u(t+N\tau_0-\tau_p) \\ +\Delta Q_B(t+N\tau_0-\tau_p)u(t+N\tau_0-\tau_p) - \Delta Q_B[t+(N-1)\tau_0]u[t+(N-1)\tau_0]h_N \end{cases};$$

$$-N\tau_o \le t \le -(N-1)\tau_o$$

where

$$h_N = \begin{cases} 1; N \ge 1 \\ 0; N = 0 \end{cases} \tag{14}$$

and the measured signal is

$$S_{AB}(t) = \sum_{N=0}^{\infty} S_{AB-N}(t) \tag{15}$$

The demodulated signal from the lock-in amplifier is the Fourier transform of the WM-DPTR signal and is expressed as in-phase ΔS_{IP} and quadrature $\Delta S_Q(\omega_o)$ channels

$$\Delta S_{IP}(\omega_o) = \frac{2}{\pi} b_1(\omega_o) \tag{16}$$

$$\Delta S_Q(\omega_o) = -\frac{2}{\pi} a_1(\omega_o)$$

with

$$\begin{bmatrix} a_1(\omega_o) \\ b_1(\omega_o) \end{bmatrix} = \frac{\omega_o}{\pi} \int_0^{\tau_o} S_{AB}(t) \begin{bmatrix} \cos(\omega_o t) \\ \sin(\omega_o t) \end{bmatrix} dt \tag{17}$$

which can be described as amplitude V_{AB} and phase P_{AB}:

$$V_{AB} = \sqrt{\Delta S_{IP}^2 + \Delta S_Q^2} \tag{18}$$

$$P_{AB} = \tan^{-1}\left(\frac{\Delta S_Q}{\Delta S_{IP}}\right)$$

As shown in Figure 14, N can have great impact on the shape of the signal waveforms of lasers A and B, especially when N is small.

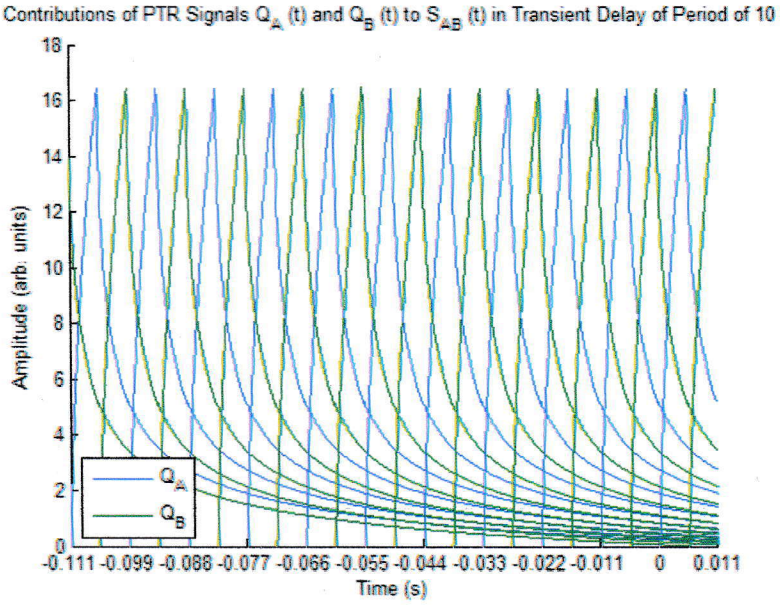
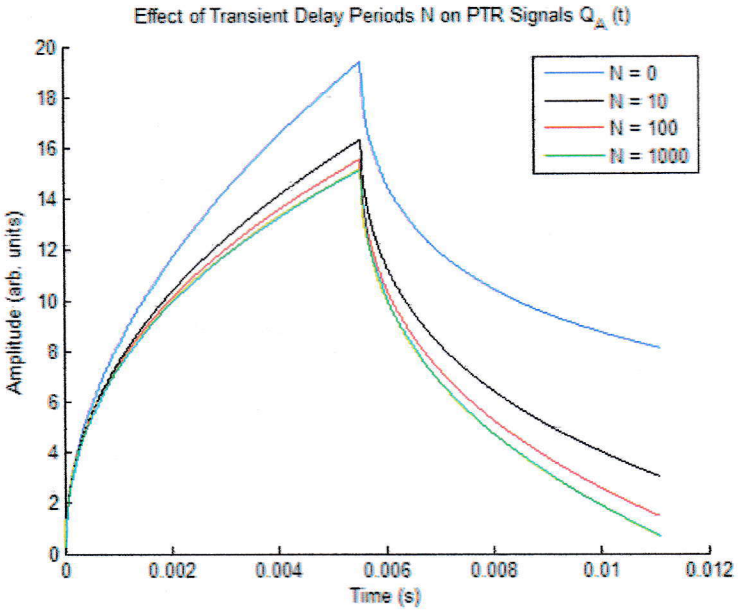
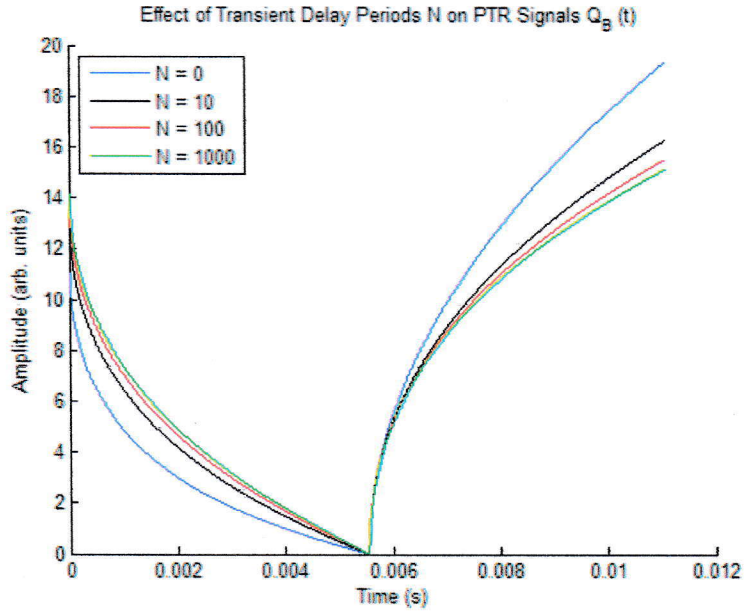


Figure 13. PTR Signals from Laser A and Laser B with Transient Delays over 10 Transient Periods



(a)



(b)

Figure 14. Effect of Transient Delay Periods N on PTR Signals from Laser A (a) Q_A (t) and Laser B (b) Q_B (t)

Chapter 4
Research Methodology

The research is completed in three phases. The first phase focuses on demonstrating the potential and feasibility of the WM-DPTR method for BAC measurement in the ethanol concentration range of 0-100 mg/dL using different ethanol phantoms. During this part of the research, the intensity ratio and phase difference combinations of the WM-DPTR system are fine-tuned for optimal ethanol phantom signal measurements. In the second phase of the research, measurement results are corroborated by simulations based on the WM-DPTR theory described above. In addition, a WM-DPTR-based calibration method is introduced and used to calibrate the developed alcohol biosensor using ethanol experimental results. Finally, the calibrated WM-DPTR-based alcohol biosensor is evaluated based on sensitivity, accuracy, precision, linearity, and measurement time.

4.1 Experimental Setup of the WM-DPTR System

The experimental setup of WM-DPTR system, illustrated in Figure 15, is described in details in [35]. The system consists of two quantum cascade lasers (QCL, 1101-95/104-CW-100-AC, Pranalytica, CA) with laser output powers of 34 mW and beam sizes ~2.5 mm emitting at two discrete wavelengths near the peak (9.5 μm or 1042 cm^{-1}) and the baseline (10.4 μm or 962 cm^{-1}) of the ethanol mid-infrared absorption band. Two function generators (33220A, Agilent Technologies, CA) produce a phase-locked square wave to modulate the laser beams and control the phase difference $dP = P_A - P_B$ between the two laser beams. To achieve ethyl alcohol detection in the ISF of the dermis layer, the laser modulation frequency which controls the probing depth is set to 90 Hz to generate a probe depth of about 40 μm in the dermis layer as illustrated in Figure 6. A motorized variable circular MIR neutral density (ND) filter (Reynard Corp, CA) is placed in front of laser B and controls the intensity ratio $R = \frac{I_A}{I_B}$ of the two lasers. The generated differential PTR infrared (thermal) photon signals, V_{AB} and P_{AB}, resulted from the two out-of-phase square-wave-modulated laser beams irradiating the sample are collected by a pair of parabolic mirrors and focused onto a HgCdZnTe detector (MCZT, PVI-4TE-5, Vigo System, Poland) with high detectivity in the 2-5 μm spectral range. The output from the MCZT

detector is then sent to the lock-in amplifier (SR850, Stanford Research Systems, CA) for demodulation. The demodulated signal is then sent back for analysis to the LabView software that is used for controlling the phase difference dP and the power ratio R of the two lasers, henceforth referred to as "the system parameters", through rotational adjustment of the neutral density filter and temporal adjustment of the two square-wave modulation waveforms.

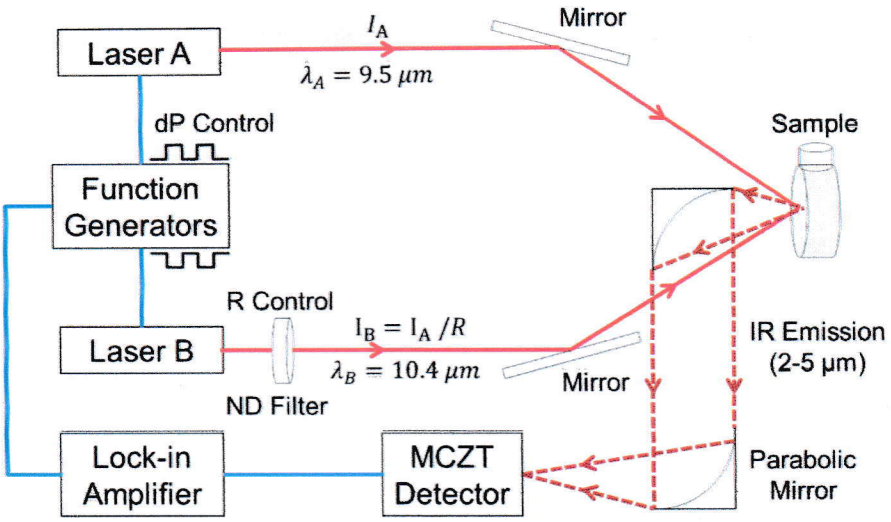


Figure 15. WM-DPTR System Configuration

4.2 Phantoms Preparation

Three types of phantoms are used for the measurements:

(1) ethanol and water,

(2) ethanol and blood serum to imitate alcohol in ISF in dermis, and

(3) ethanol diffused from skin samples for closest simulation of actual field measurement conditions.

The simplified phantom 1 was used first for initial feasibility study of using WM-DPTR method in ethanol measurement. Human serum was chosen for phantom 2 because it is a good alternative to ISF [18]. Phantom 3 allows for closest simulation to actual field measurement conditions.

To prepare phantom 1, the first step was to prepare 50 mL ethanol-water solution for each of the ethanol concentration to be measured. The process was as follows:

1. Add about 25 mL of deionized water to a 50 mL volumetric flask
2. Add the appropriate amount of pure ethanol (GreenField Ethanol Inc. ON, Canada), as indicated in Table 3 to the volumetric flask using a micropipette by immerging the pipette tip in the water and then releasing the ethanol
3. Fill the volumetric flask with deionized water to the red mark using a transfer pipette
4. Seal the volumetric flask with a rubber stopper and shake the flask to obtain homogeneous solution

Table 3. Amount of Pure Ethanol Added to Solution for Obtaining a Given Ethanol Concentration

Ethanol Concentration (mg/dL)	**Amount of Pure Ethanol** (uL)
0	0
40	25.4
80	50.7
120	76.1
160	101.4
200	126.7

For phantom 2, human blood serum (Catalog number 1016011, American Biological Technologies Inc. TX) was mixed with ethanol instead of water. To prepare phantom 3, the following additional steps were taken:

- Remove ZnSe window from the cuvette
- Cut the 1 mm thick skin, obtained from TMB cosmetic tummy tuck abdominal plastic surgery with the approval of the Research Ethics Office of the University of Toronto, into a circular shape of about 25 mm diameter
- Glue the skin onto the cuvette with the stratum corneum layer facing the laser beam, as depicted in Figure 16.

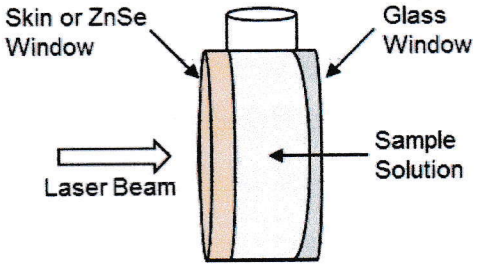


Figure 16. Diagram of the Cuvette

4.3 Ethanol Measurement Procedure

Ethanol measurements were performed as follows:

1. Phantoms containing different concentrations of ethanol were first prepared.
2. Before measurement, the prepared solution was transferred to the cuvette using a transfer pipette. Ethanol measurements were conducted in increasing ethanol concentration starting with water.
3. The cuvette was then placed in the sample holder of the WM-DPTR system.
4. The WM-DPTR system was tuned to different system parameter combinations for ethanol measurement.
5. After ethanol measurements, the cuvette was removed from the system and a small sample from the cuvette was transferred using the transfer pipette to a micro-tube using which the ethanol concentration of the solutions was verified with a biochemistry analyzer (YSI 2700S, Life Sciences, OH).
6. The cuvette was then emptied and rinsed with ethanol with the same concentration as the next solution.
7. Steps 2-5 were repeated for the remaining solutions.

To avoid contamination, a different transfer pipette and tip of the transfer pipette was used for each solution.

4.4 Simulations of WM-DPTR System

Based on the WM-DPTR theory described in Chapter 3, ethanol detection using WM-DPTR was simulated through programming in MATLAB with the differential amplitude and phase determined using Equation 18. The simulations were focused on solutions with 0-120 mg/dL of ethanol. In the simulation, the samples were considered to be excited using two out-of-phase laser beams of wavelengths at the peak (9.5 um) and at the baseline (10.4 um) of the ethanol absorption band. The IR detector band was set to 2-5 um which is consistent with the mid-infrared detector used during ethanol measurements.

Like the ethanol measurement, the modulation frequency or $1/\tau_o$was set at 90 Hz. The two system parameters in the simulations, as in the experimental work, are amplitude ratio R, which is defined as the ratio of pure water PTR amplitudes generated from laser A and laser B alone or $R = A_{AW}/A_{BW}$, and phase shift dP, which is phase difference between water PTR phases generated from lasers A and B alone or $dP = P_{AW} - P_{BW}$. Amplitude ratio R is normally set in the neighborhood of 1 by adjusting the laser intensities of I_{OA} and I_{OB} while phase shift is normally set around 180 by adding a time delay of lead Δt to the PTR signal from laser B or $S_B(t) = S_B(t + \Delta t)$. $K(\lambda_1, \lambda_2)$ was set to 0.0364 W $K^{-1}cm^{-3}$, the same value used for WM-DPTR simulation on water-glucose mixtures. The fitting parameter $\bar{\mu}_{IR}$ was varied from 0 to 1000 cm^{-1} to obtain the best fit. This is accomplished by finding the value that gives the minimum mean square error (MMSE) between the calibration curves and ethanol measurement results, optimizing the fitting parameter in the whole range of 0-100 mg/dL. The optimization could be performed for bundled ranges of interest by the sensitivity tunability property. $\bar{\mu}_{IR}$ values applied are 237 cm^{-1} for phantom 1, 158 cm^{-1} for phantom 2, and 141 cm^{-1} for phantom 3. Since the time constant set on the lock-in amplifier is 10 seconds, prior transients delay period number N is set to 1000.

Appropriate equations were used to model the optical and thermal properties of the sample. The absorption coefficient of the sample was calculated from [36]

$$\mu_e = \sum_i v_i \mu_{e,i} \tag{19}$$

where $\mu_{eA,i}$ is the absorption coefficient of the pure component i and v_i is the volume fraction of the pure component i. The thermal conductivity was computed from [37]

$$k = \sum_i v_i k_i \tag{20}$$

where k_i is the thermal conductivity of the pure component i. The thermal diffusivity was determined from [38]

$$\alpha = \frac{k}{\rho c} = \frac{k}{\sum_i v_i \rho_i c_i} \tag{21}$$

where ρc is the product of density and specific heat capacity of the sample, ρ_i is the density of the pure component i, and c_i is the specific heat capacity of the pure component i. The components in the model consist of ethanol, blood serum, and skin. 70.2% is used as the volume fraction of water in the dermis in the simulations [39].

Values for the thermal and optical properties of ethanol, water, serum, and skin used in the simulator were drawn from various sources. The ethanol absorption coefficient was obtained from NIST Chemistry WebBook [40], the water spectrum from Wieliczka *et al.* [41], and the thermal properties of ethanol-water from measurements by Wang and Fiebig [42]. As for skin data, the thermal properties are obtained from the paper by Dai et al. [43] and the optical properties from Michel *et al.* [44]. In the case of human serum, the thermal properties are based on data on IT'IS Foundation database [45] and optical properties on work done by Giovenale et al [46]. Tables 4-6 list the thermal and optical properties of the three phantoms used for

increasing ethanol concentrations. For all ethanol concentrations, the absorption coefficient μ_{eB} is 735.5 cm^{-1} for phantom 1, 806.5 cm^{-1} for phantom 2, and 1036.5 cm^{-1} for phantom 3.

Table 4. Optical and Thermal Property Changes with Varying Ethanol Concentration in Ethanol and Water Solutions

C_{ETOH} (mg/dL)	μ_{eA} (cm^{-1})	k (10^{-3} W/cm K)	α (10^{-3} cm^2/s)
0	531.1	5.967	1.4190
20	531.0	5.965	1.4187
40	530.9	5.964	1.4184
60	530.8	5.963	1.4180
80	530.8	5.961	1.4177
100	530.7	5.960	1.4174
120	530.6	5.959	1.4170

Table 5. Optical and Thermal Property Changes with Varying Ethanol Concentration in Ethanol and Serum Solutions

C_{ETOH} (mg/dL)	μ_{eA} (cm^{-1})	k (10^{-3} W/cm K)	α (10^{-3} cm^2/s)
0	602.1	5.200	1.3695
20	602.0	5.199	1.3694
40	601.9	5.198	1.3694
60	601.8	5.197	1.3693
80	601.7	5.195	1.3692
100	601.6	5.194	1.3691
120	601.5	5.193	1.3690

Table 6. Optical and Thermal Property Changes with Varying Ethanol Concentration in Human Serum Solutions Diffused through Skin

C_{ETOH} (mg/dL)	μ_{eA} (cm^{-1})	k (10^{-3} W/cm K)	α (10^{-3} cm^2/s)
0	832.1	5.230	1.3231
20	832.0	5.229	1.3230
40	831.9	5.228	1.3229
60	831.8	5.227	1.3229
80	831.7	5.227	1.3228
100	831.6	5.226	1.3228
120	831.5	5.225	1.3227

4.5 Calibration Curves and Ethanol Evaluation

The simulated ethanol measurement curves can be used as calibration curves using which ethanol concentration can be converted from experimentally measured amplitude and phase values. By comparing the estimated with actual ethanol concentration, one can determine the accuracy and precision of the alcohol sensor through an ethanol estimation algorithms. The performance of the WM-DPTR can vary depending on the calibration method used. The calibration methods, ethanol estimation algorithms, and WM-DPTR-based ethanol biosensor details are given in Chapter 6.

Chapter 5
Experimental and Simulation Results, Analysis, and Discussion

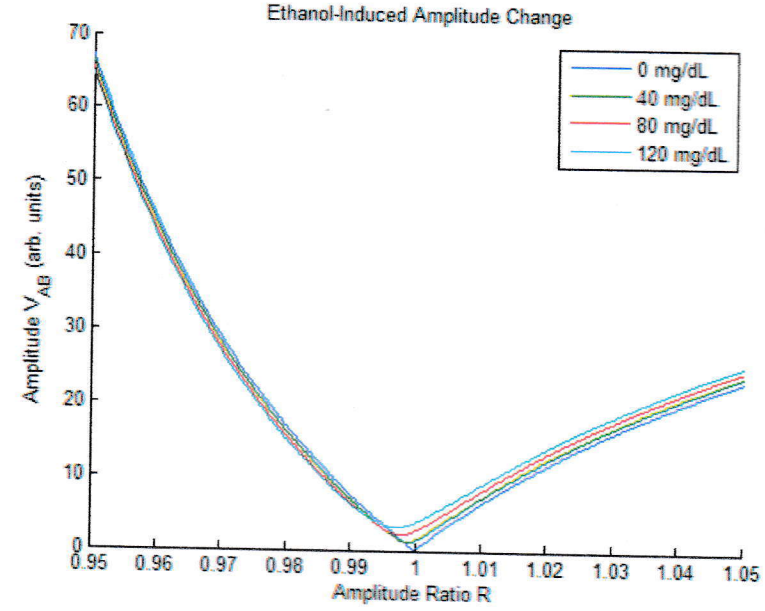
Measurements were performed using different phantoms with various system parameter combinations to explore the BAC measurement sensitivity and linearity of WM-DPTR for each phantom. In the graphs in this chapter, V_{AB} and P_{AB} represent the voltage and phase of the differential signal at the output of the lock-in amplifier.

For each data point, five sequential measurements were taken and averaged. The error bars represent the standard deviation of the five measurements. Linear regression was applied for the entire 0-110 mg/dL ethanol concentration range and for specific ethanol concentration range. The sensitivity of BAC measurements can be determined from the slope of linear regression with units of μV per mg/dL for amplitude and degree per mg/dL for phase. The correlation coefficient can be used to determine the linearity of the developed biosensor.

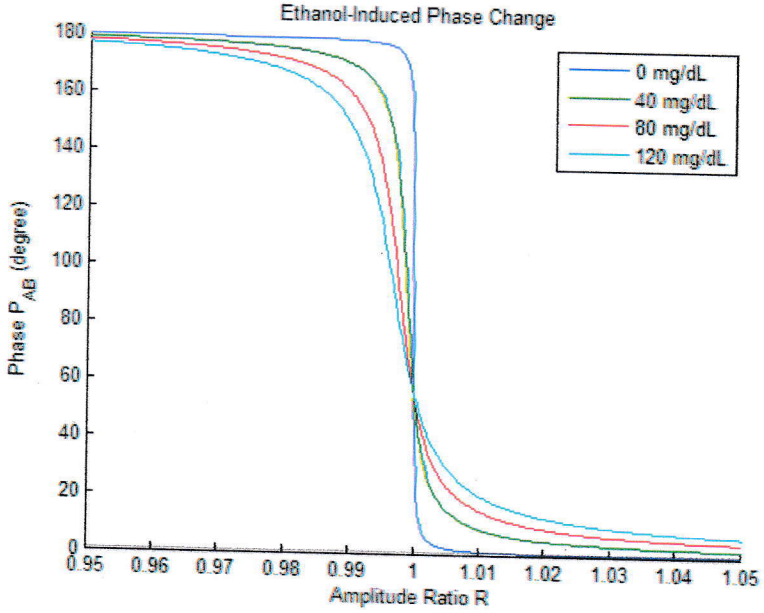
5.1 Characteristics of the WM-DPTR system

To highlight the characteristics of the WM-DPTR system, initial simulations were done using phantom 1 (ethanol and water solutions). For phase difference dP less than 180, the resultant amplitude and phase signals versus different amplitude ratio R at different ethanol concentration, namely 0, 40, 80, and 120 mg/dL, are plotted in Figure 17.

In Figure 17a, as ethanol concentration increases, the set of V curves become rounded off and rises due to the phase shift deviation caused by ethanol concentration. One can note that the V curves are not symmetric about R = 1 with the troughs of the V curves shifting toward smaller R, allowing for a larger dynamic range in the region of R > 1. The amplitude is not monotonic with the region of R < 1 exhibiting a lower resolution.



(a)



(b)

Figure 17. Amplitude Ratio R Dependence of WM-DPTR Signal at Different Ethanol Concentrations (a) Ethanol-Induced Differential Amplitude Change (b) Ethanol-Induced Differential Phase Change

The phase transition or the Z curves, as illustrated in Figure 17b, becomes more gradual with increased ethanol concentration due to the phase shift deviation. Unlike amplitude, its resolution is lower in the region of $\bar{R} > 1$, indicating that the ethanol detection sensitivity of WM-DPTR is

amplitude ratio dependent and the amplitude and phases are complementary. The crossing point is below the midpoint, allowing a greater dynamic range in the region of R < 1.

5.2 Phantom 1 – Water and Ethanol Solutions

Table 7 contains the ethanol measurement results for phantom 1 with Standard Deviation (SD) of the five measurements.

The differential amplitude V_{AB} increases by 15% with the system parameter combinations of (R = 1.02, dP = 180.31°) and the differential phase P_{AB} changes by 9% with (R = 0.99 and dP = 180.32°).

Table 7. WM-DPTR Ethanol Measurement – Phantom 1

Ethanol Concentration (mg/dL)	Amplitude (uV)	SD Amplitude	Phase (°)	SD Phase
0	4.106	0.002	225.574	0.196
22.7	4.339	0.005	223.079	0.054
40.9	4.537	0.004	220.768	0.091
65.7	4.635	0.004	216.574	0.136
108.7	4.727	0.002	205.957	0.049

If a linear regression is applied on the experimental data, for differential amplitude and phase measurements, the overall sensitivity is 0.0050 μV per mg/dL and 0.18° per mg/dL respectively and the overall correlation coefficient is 0.9336 and 0.9842 respectively. In addition, the error bars showing standard deviation of the five measurements are very small that they are hard to see, implying high measurement precision of WM-DPTR system.

The measurement data can be analyzed using a piecewise approach where linear regression is applied for a range of ethanol concentration. For the range of ethanol concentration of 0-40.9 mg/dL, the differential amplitude measurement exhibits a sensitivity of 0.011 μV per mg/dL and linearity of 0.9998 in correlation coefficient while the differential phase measurement exhibits a sensitivity of 0.12° per mg/dL and linearity of 0.9991 in correlation coefficient. For the range of

ethanol concentration of 40.9-108.7 mg/dL, for differential amplitude measurements, the sensitivity is 0.0027 μV per mg/dL and the linearity in 0.9852 and, for differential phase measurements, the sensitivity is 0.22° per mg/dL and the linearity is 0.9958. This illustrates that the right selection of system parameter combinations of R and dP renders amplitude and phase complementary in that amplitude is more sensitive in the low concentration range while phase is more sensitive in the high concentration range and that better linearity and sensitivity can be achieved when a piecewise approach is applied.

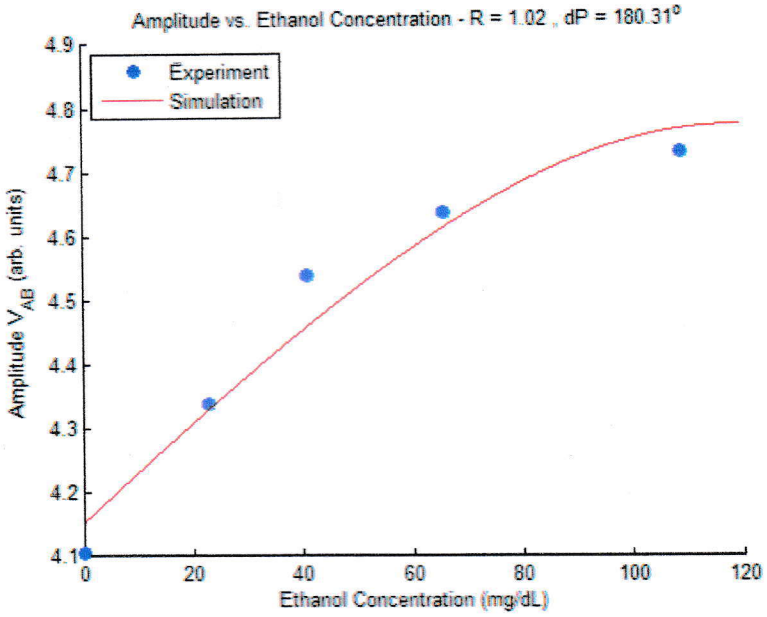
From Figure 18, the simulation and experimental results have similar overall curve shape. The amplitude of the differential signal increases monotonically with increasing ethanol concentration and the phase decreases monotonically with increasing ethanol concentration. One can also observe, for amplitude of the differential signal, higher sensitivity for low ethanol concentrations and lower sensitivity for high ethanol concentrations, and, for phase of the differential signal, higher sensitivity for high ethanol concentrations and lower sensitivity for low ethanol concentrations. The mean error between them is about 0.036 μV with a percent error of 0.88% for differential amplitude measurement and 0.057° with a percent error of 0.025% for differential phase measurement.

5.3 Phantom 2 – Blood Serum and Ethanol Solutions

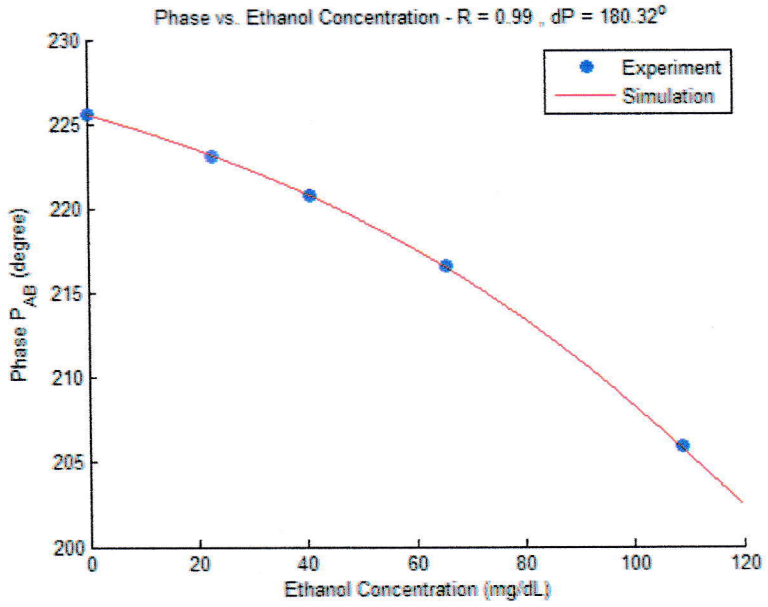
From Table 8 where the ethanol measurement results for blood serum and ethanol solutions are shown, the differential amplitude V_{AB} decreases by 30% with system parameter combination of (R = 0.98, dP = 180.37°) and the differential phase P_{AB} decreases by 10% with (R = 0.99, dP = 180.36°). The large change in both amplitude and phase values with varying ethanol concentrations indicates that the WM-DPTR measurements of ethanol concentrations are well-resolved in the 0-100 mg/dL range.

For differential amplitude measurements, the overall sensitivity is 0.0094 μV per mg/dL with a correlation coefficient of 0.9302. The sensitivity and correlation coefficient for differential phase measurements is higher, 0.23° per mg/dL for sensitivity and 0.9483 for correlation coefficient. Like the measurement results with phantom 1, the ethanol concentrations are well-resolved with

amplitude and phase and the standard deviation of the five measurements are fairly small, implying, again, high measurement precision of WM-DPTR system.



(a)



(b)

Figure 18. Measured and Simulated WM-DPTR Signals with Ethanol and Water Solutions (a) Differential Amplitude Measurement (b) Differential Phase Measurement

A piecewise approach is also taken when analyzing the measurement data. The differential amplitude measurement exhibits a sensitivity of 0.016 μV per mg/dL for the range of ethanol concentration of 0-46.7 mg/dL and 0.0041 μV per mg/dL for the range of ethanol concentration of 46.7-103 mg/dL and a linear correlation coefficient of 0.9997 for the range of ethanol concentration of 0-46.7 mg/dL and 0.8950 for the range of ethanol concentration of 46.7-103 mg/dL. As for differential phase measurements, the sensitivity achieved is 0.36° per mg/dL for the range of ethanol concentration of 0-46.7 mg/dL and 0.12 ° per mg/dL for the range of ethanol concentration of 46.7-103 mg/dL and the linear correlation coefficient is 0.9995 for the range of ethanol concentration of 0-46.7 mg/dL and 0.9611 for the range of ethanol concentration of 46.7-103 mg/dL.

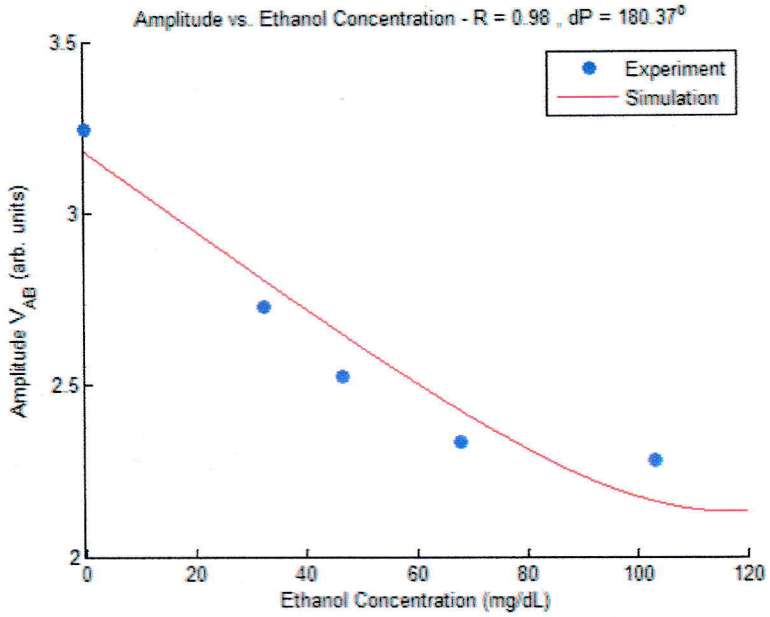
Table 8. WM-DPTR Ethanol Measurement – Phantom 2

Ethanol Concentration (mg/dL)	Amplitude (uV)	SD Amplitude	Phase (°)	SD Phase
0	3.243	0.015	241.151	0.055
32.5	2.728	0.006	229.081	0.037
46.7	2.525	0.002	224.490	0.094
67.9	2.332	0.002	220.163	0.585
103	2.280	0.003	217.514	0.059

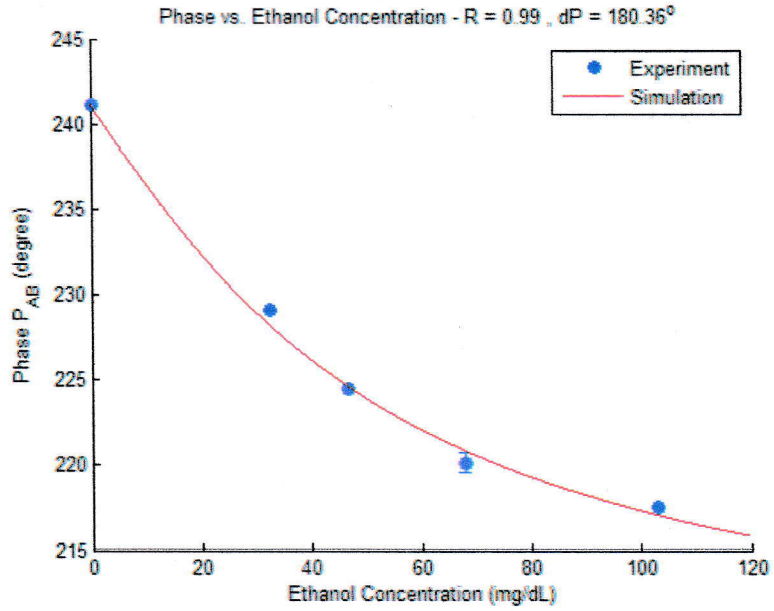
Comparing the simulation results, displayed in Figure 19, with the experimental results, the mean error between them is about 0.095 μV, a percent error of 3.8%, for differential amplitude measurement and 0.43 degree for differential phase measurement, a percent error of 0.19%. Both amplitude and phase of the differential signal decrease monotonically with increasing ethanol concentration. For differential amplitude and phase, both simulation and experimental results suggest that the phase is more sensitive in the low concentration range.

5.4 Phantom 3 – Ethanol and Serum Diffused from Skin

To simulate more closely to in vivo WM-DPTR measurements, for each load of new solution, a 25-minute wait time was applied before starting measurements for phantom 3 so that the sample solution could reach equilibrium through diffusion with the skin window. The ethanol measurements with phantom 3 are shown in Table 9.



(a)



(b)

Figure 19. Measured and Simulated WM-DPTR Signals with Ethanol and Serum Solutions (a) Differential Amplitude Measurement (b) Differential Phase Measurement

For the given system parameter combinations of (R = 0.99, dP = 179.68) for differential amplitude and (R = 0.96, dP = 179.53) for differential phase, the differential amplitude V_{AB} decreases by about 43% and the differential phase P_{AB} increases by 80%. Thus, WM-DPTR

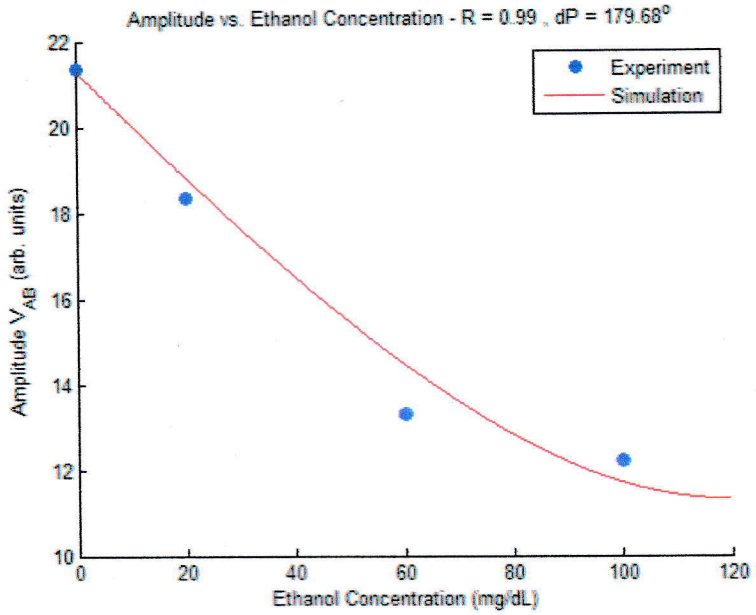
measurements of ethanol concentrations in the 0-100 mg/dL range are well-resolved both with amplitude and phase for phantom 3.

Table 9. WM-DPTR Ethanol Measurement – Phantom 3

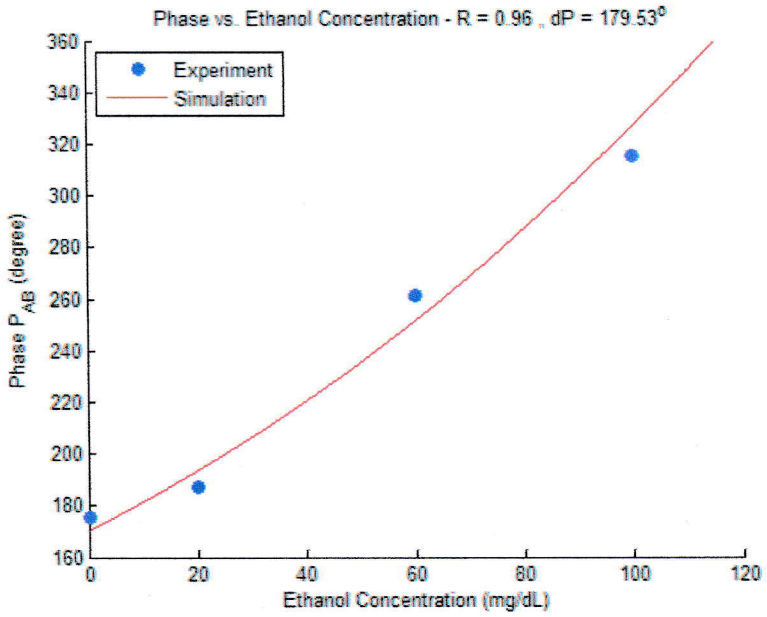
Ethanol Concentration (mg/dL)	Amplitude (uV)	SD Amplitude	Phase (°)	SD Phase
0	21.364	0.024	175.382	0.325
20	18.335	0.033	187.045	0.448
60	13.276	0.059	261.402	0.924
100	12.184	0.026	315.029	0.416

After applying linear regression on the experimental data, the system's overall sensitivity is 0.093 μV per mg/dL and 1.47° per mg/dL and correlation coefficient is 0.9588 and 0.9927 for amplitude and phase measurements respectively. Moreover, from the error bars shown, the standard deviations of the ethanol measurements are very small, implying high measurement precision.

Like the previous two phantoms, the measurement data is analyzed using a piecewise approach. The differential amplitude exhibits a sensitivity of 0.13 μV per mg/dL and linearity of correlation coefficient of 0.9989 for the range of ethanol concentration of 0-60 mg/dL and a sensitivity of 0.027 μV per mg/dL for the range of ethanol concentration of 60-100 mg/dL. For the differential phase, the system can achieved a sensitivity of 0.58° per mg/dL for the range of ethanol concentration of 0-20 mg/dL and a sensitivity of 1.60° per mg/dL and a correlation coefficient of 0.9956 for the range of ethanol concentration of 60-100 mg/dL. Here, one can observe again that amplitude is more sensitive in the low concentration range while phase is more sensitive in the high concentration range, underlining amplitude and phase complementary property of the WM-DPTR system. As illustrated in the previous two phantoms, better linearity and sensitivity can be achieved when performing analysis with a piecewise approach.



(a)



(b)

Figure 20. Measured and Simulated WM-DPTR Signals with Ethanol and Human Serum Solutions Diffused through Skin (a) Differential Amplitude Measurement (b) Differential Phase Measurement

The simulation results are close to experimental results as illustrated in Figure 20. The amplitude of the differential signal decreases monotonically with increasing ethanol concentration and the phase decreases monotonically with increasing ethanol concentration. The

average error between the simulation and experiment results is about 0.55 μV with a percent error of 3.9% for the differential amplitude and 8.3° with a percent error of 3.5% for the differential phase. Like phantom 2, both simulation and experimental results suggest that the differential amplitude is more sensitive in the low concentration range while the differential phase is more sensitive in the high concentration range.

To explore the sensitivity tunability property of WM-DPTR, ethanol measurements were performed with various system parameter combinations of R and dP. Table 10 contains the experimental and simulation results of differential phase with system parameter combinations (R = 0.96, dP = 179.56). Like previous measurement results, the standard deviations of the ethanol measurements are very small, implying high measurement precision.

Although the sensitivity for the ethanol concentration range of 0-60 mg/dL is not as high as with system parameter combination of (R = 0.96, dP = 179.53), the WM-DPTR system has higher sensitivity, 2.66° per mg/dL, in the 60-100 mg/dL ethanol concentration range in which the phase plunges by about 106°. Given that the legal limit is 80 mg/dL, these WM-DPTR settings (R = 0.96 and dP = 179.56) are useful for quick roadside pass or fail alcohol tests. As depicted in Figure 21, the simulation results are similar to experimental results with a mean error of 3.4° and mean percentage error of 2.3%. Like the experimental results, the simulation results also indicate higher sensitivity in the high concentration range.

Table 10. WM-DPTR Ethanol Measurement for Quick Roadside Alcohol Tests

Ethanol Concentration (mg/dL)	Phase (°)	SD Phase
0	158.504	0.334
20	158.471	0.021
60	126.770	0.837
100	20.333	0.185

The experimental results for quick roadside alcohol tests underscore the sensitivity tunability property of WM-DPTR since, by varying system parameter combinations of R and dP, the WM-

DPTR can increase sensitivity for a particular range of ethanol concentrations. In this case, the system achieves a very high sensitivity in the ethanol concentration range of 60-100 mg/dL.

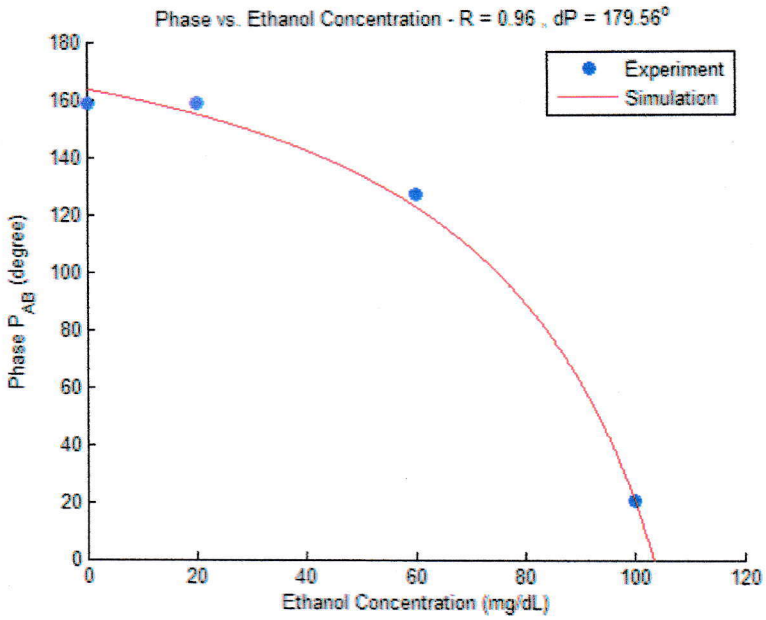


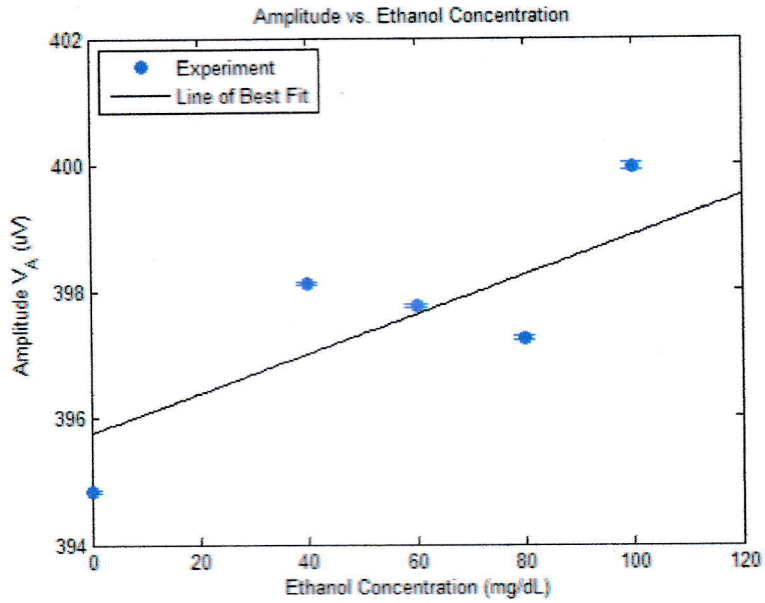
Figure 21. WM-DPTR Phase Ethanol Measurement and Simulation – Quick Roadside Alcohol Tests

5.5 Ethanol Measurements with Single-PTR

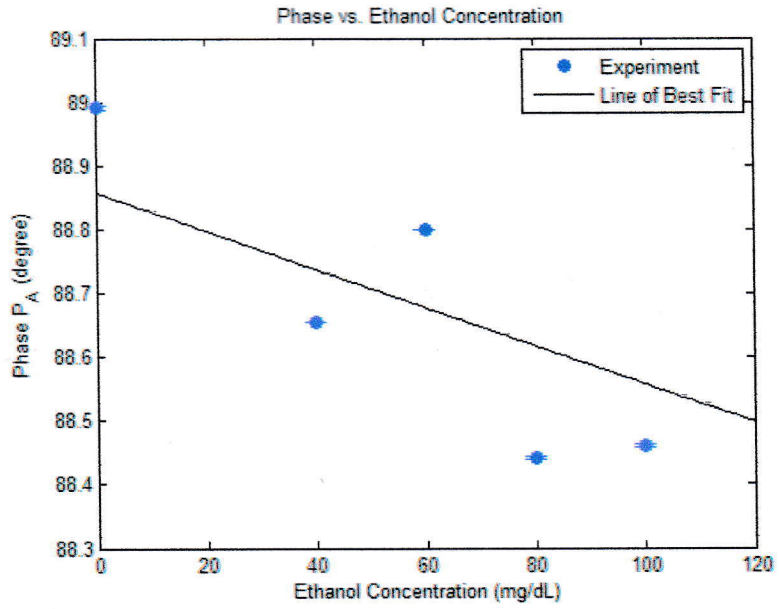
To highlight the advantages of the differential WM-DPTR method compared with the conventional single-ended PTR methods, ethanol measurements are performed using phantom 3, ethanol and serum diffused from skin, using single laser A with operating wavelengths at the peak of the ethanol absorption spectrum. The results are shown in Table 11 and Figure 22.

Table 11. Single-Ended Ethanol Measurement – Phantom 3

Ethanol Concentration (mg/dL)	Amplitude (uV)	SD Amplitude	Phase (°)	SD Phase
0	394.841	0.016	88.991	0.003
40	398.113	0.027	88.656	0.000
60	397.761	0.016	88.800	0.000
80	397.249	0.034	88.441	0.003
100	399.955	0.054	88.460	0.003



(a)



(b)

Figure 22. Single-Ended PTR Measurements with Phantom 3 (a) Single-Ended PTR Amplitude Measurements (b) Single-Ended PTR Phase Measurement

For the ethanol concentration range of 0-100 mg/dL, the amplitude V_A signal only increases by 1.7% and the phase P_A only decreases by 0.7%. In addition, for amplitude and phase

measurements, the overall sensitivity is 0.031 μV per mg/dL and 0.0030° per mg/dL respectively and the correlation coefficient is 0.9142 and 0.8355 respectively. Thus, the sensitivity from the single-ended PTR measurements is too low for ethanol measurements below 100 mg/dL. Moreover, the increase in amplitude and decrease in phase due to increasing ethanol concentration are not monotonic. All of the above observations indicate that single-ended PTR methods are impractical for accurate and precise ethanol sensing.

5.6 Experimental and Simulation Results Discussion

5.6.1 Comparison between Single-Ended PTR and WM-DPTR Method

To compare measurement results from single-ended PTR with WM-DPTR method, the measurement results from both methods are listed in Tables 12-14.

As one may observe, both the sensitivity and linearity improve dramatically, by more than a factor of 3 for sensitivity, if BAC is measured using the differential method. This is because, although the optical absorption of ethanol is highest at 9.5 μm, the water optical absorption is also high. This means that the single-ended PTR system depends more on the thermal properties of ethanol to measure the ethanol concentration and, as one can observe from Table 4-Table 6, the changes in optical properties due to varying ethanol concentrations are greater than the changes in thermal properties. Thus, the sensitivity is reduced when the single-ended PTR method is employed. In addition, the differential method removes confounding interference such as skin pigments and other baseline variations, which leads to higher linearity.

5.6.2 Dual Channel Measurements and Simulations

The WM-DPTR method allows for dual channel measurements: amplitude and phase. Comparing the sensitivity and linearity of amplitude and phase measurements for all phantoms, the relationship between P_{AB} and ethanol concentration is more linear and the sensitivity of the ethanol measurement from the phase channel is higher. The above observations are in line with simulation results. One explanation is that the amplitude is more susceptible to environmental

noise; the precision and accuracy in the amplitude channel of the lock-in amplifier is lower than that of the phase channel, as described in Table 15.

In general, the simulation predicts the alcohol measurement results with good accuracy. Table 16 contains the mean error and mean percent error between the simulation and experimental results.

Table 12. Sensitivity of WM-DPTR-Based Alcohol Biosensor

	Channel	**Ethanol Concentration Range (mg/dL)**					
		~0-100	~0-20	~20-40	~40-60	~60-80	~80-100
Phantom 1	Amplitude	0.0050	0.011	0.011	0.0027	0.0027	0.0027
	Phase	0.18	0.12	0.12	0.22	0.22	0.22
Phantom 2	Amplitude	0.0094	0.016	0.016	0.0041	0.0041	0.0041
	Phase	0.23	0.36	0.36	0.12	0.12	0.12
Phantom 3	Amplitude	0.093	0.13	0.13	0.13	0.027	0.027
	Phase	1.47	0.58	0.58	1.60	1.60	1.60
Road Test	Phase	1.37	0.57	0.57	0.57	2.66	2.66
Units for amplitude sensitivity: μV per mg/dL Units for phase sensitivity: ° per mg/dL							

Table 13. Linearity of WM-DPTR-Based Alcohol Biosensor

	Channel	**Ethanol Concentration Range (mg/dL)**					
		~0-100	~0-20	~20-40	~40-60	~60-80	~80-100
Phantom 1	Amplitude	0.9336	0.9998	0.9998	0.9852	0.9852	0.9852
	Phase	0.9842	0.9991	0.9991	0.9958	0.9958	0.9958
Phantom 2	Amplitude	0.9302	0.9997	0.9997	0.8950	0.8950	0.8950
	Phase	0.9483	0.9995	0.9995	0.9611	0.9611	0.9611
Phantom 3	Amplitude	0.9588	0.9989	0.9989	0.9989		
	Phase	0.9927			0.9956	0.9956	0.9956
Road Test	Phase	0.9263	0.9452	0.9452	0.9452		
Note: Correlation coefficient for shaded ones is 1 because the mathematical model is based on two data points.							

Table 14. Sensitivity and Linearity of Single-Ended PTR Alcohol Biosensor

	Channel	**Single Laser**	
		Sensitivity	**Linearity**
Phantom 3	Amplitude	0.031	0.9142
	Phase	0.0030	0.8455

Table 15. Error and Sensitivity of Lock-in Amplifier [47]

Channel	Sensitivity	Error
Amplitude	2 nV	±1 % (±0.2 % typically)
Phase	0.001°	> 0.001° (relative) > 1° (absolute)

Table 16. Mean Error and Percent Error between Simulation and Experimental Results

	Channel	Mean Error	Mean Percent Error
Phantom 1	Amplitude	0.036 μV	0.88%
	Phase	0.057°	0.025%
Phantom 2	Amplitude	0.095 μV	3.8%
	Phase	0.43°	0.19%
Phantom 3	Amplitude	0.55 μV	3.9%
	Phase	8.3°	3.5%
Road Test	Phase	3.4°	2.3%

The mean percent error between simulation and experimental results is less than 4% for all cases. One can note that the mean percent error is less for the phase channel compared to the amplitude channel. One reason is due to the age of the lasers. It was noticed during experiment that the laser intensity fluctuated with the change in the room temperature; laser intensity has greater influence on the amplitude of the signal than the phase. With new lasers, the simulation and experimental is expected to be aligned more closely.

Chapter 6
Calibration and Evaluation of the Developed Alcohol Biosensor

In Chapter 5, the sensitivity and linearity of the WM-DPTR-based alcohol biosensor were analyzed since sensitivity of a biosensor is a way to measure the sensing capability of a biosensor while high linearity allows for best interpolation. As shown in Table 12 and Table 13, the developed WM-DPTR-based alcohol biosensor can achieve an overall sensitivity of 0.093 μV per mg/dL for differential amplitude and 1.47° per mg/dL for differential phase and an overall linearity of 0.9588 for differential amplitude and 0.9927 for differential phase. This is comparable to other developed such as the one from Şenol Alpat and Azmi Telefoncu which have a correlation coefficient of 0.9984 and a sensitivity of 422.43 μA per mM or 0.0917 μA per mg/dL [48].

In terms of measurement time, for ethanol measurements using the WM-DPTR-based biosensor, a large (10 s) time constant was applied to ensure signal stability since aged lasers were used during the measurement, leading to long delay in lock-in amplifier steady measurements and resulting in a measurement time of about 2 minutes. This record can be vastly improved with state-of-art QCL technology.

In the remaining of this chapter, the developed alcohol biosensor is calibrated using two different approaches. The calibrated alcohol biosensor performance in terms of accuracy, precision, and measurement time from the two calibration approaches is discussed.

6.1 Ethanol Concentration Estimation from Calibration Curves

The developed ethanol concentration estimator uses the ethanol calibration curves to estimate BAC based on both measured amplitude and phase. The estimator takes the following steps to determine BAC:

1. Estimate ethanol concentration using amplitude calibration curve ($BAC_{amplitude}$)
2. Estimate ethanol concentration using phase calibration curve (BAC_{phase})

3. Determine estimated ethanol concentration range (BAC_{range}) using average of $BAC_{amplitude}$ and BAC_{phase}

   If BAC_{range} <= Threshold → Low ethanol concentration range

   If BAC_{range} > Threshold → High ethanol concentration range

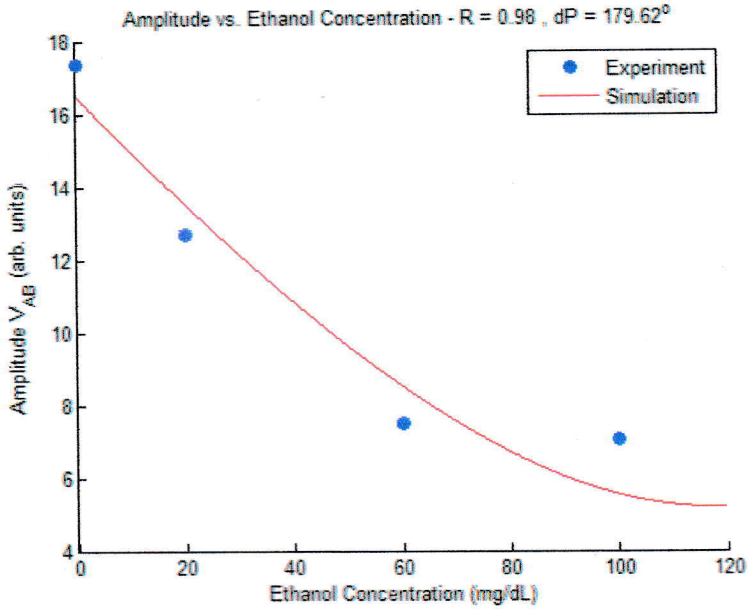
4. Take weighted average of $BAC_{amplitude}$ and BAC_{phase} to obtain estimated ethanol concentration using Equation 19. The weighting β depends on the estimated ethanol concentration range.

$$BAC = \beta \cdot BAC_{amplitude} + (1 - \beta) \cdot BAC_{phase} \quad (22)$$

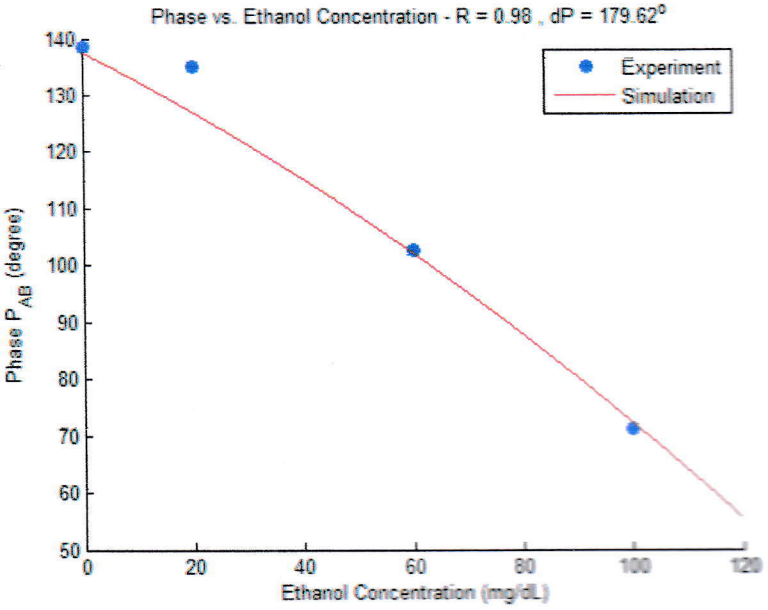
This ethanol concentration estimator takes takes advantage of the WM-DPTR amplitude and phase complementary sensitivity to optimize the accuracy and precision of the developed biosensor. When taking the weighted average of $BAC_{amplitude}$ and BAC_{phase} to estimate BAC, more weight is applied to $BAC_{amplitude}$ if the estimated BAC is in the low ethanol concentration range where the amplitude channel has higher sensitivity and more weighting to BAC_{phase} if the estimated BAC is in the high ethanol concentration range where the phase channel has higher sensitivity. A threshold value is used to determine these low and high ethanol concentration ranges. Setting the threshold value to 50 BAC gave the best results.

6.2 Calibration and Evaluation with Common $\bar{\mu}_{IR}$ for Amplitude and Phase

In the first alcohol biosensor calibration approach, a single fitting parameter value $\bar{\mu}_{IR}$ is obtained for both amplitude and phase for the best fit of the experimental data to WM-DPTR theory. $\bar{\mu}_{IR}$ values were swept from 1 to 1000 and, for each $\bar{\mu}_{IR}$ value, the mean square error (MSE) between the calibrated curve and the experimental results was calculated. It was found that MMSE is achieved when $\bar{\mu}_{IR} = 141\ cm^{-1}$. Calibration curves were obtained for two sets of system parameter combinations and are shown in Figure 23 and Figure 24. After varying β between 0 to 1, it was found that the smallest mean error and mean variance was obtained when setting β to 0.74 for low ethanol concentrations and 0.06 for high ethanol concentrations. The ethanol concentration estimation results are given in Table 17 and Table 18.

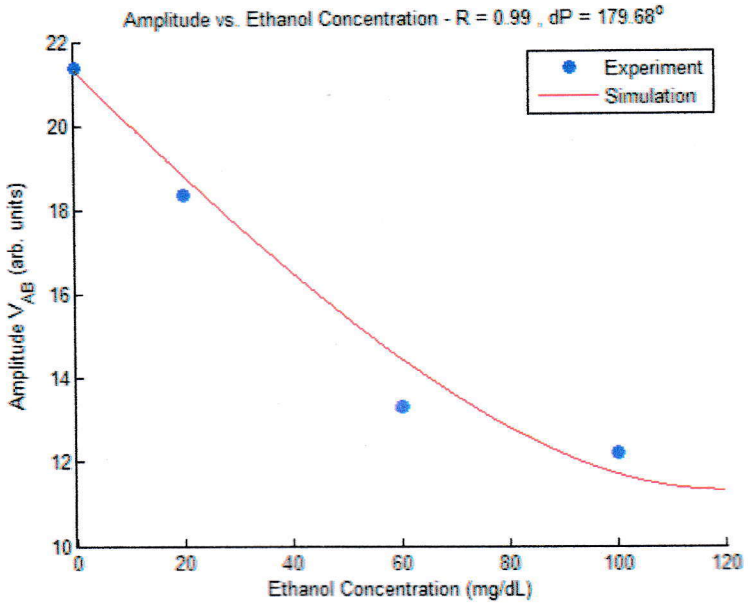


(a)

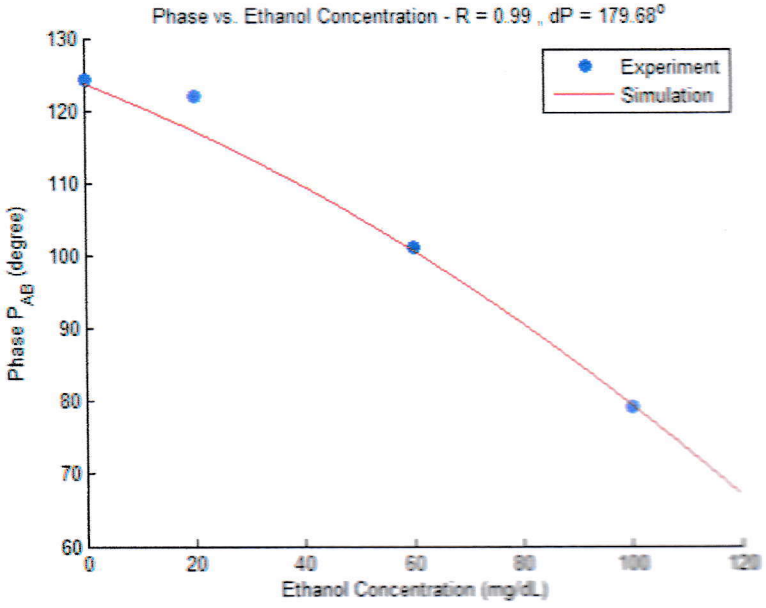


(b)

Figure 23. Ethanol Calibration Curves Using a Common Fitting Parameter Value for Amplitude and Phase with the System Parameter Combination of R = 0.98, dP = 179.62°: (a) Differential Amplitude and (b) Differential Phase



(a)



(b)

Figure 24. Ethanol Calibration Curves Using a Common Fitting Parameter Value for Amplitude and Phase with the System Parameter Combination of R = 0.99, dP = 179.68°: (a) Differential Amplitude and (b) Differential Phase

Using this approach, ethanol concentration estimation using WM-DPTR system parameter combination of (R = 0.99, dP = 179.68°) yields better results than with (R = 0.98, dP = 179.62°). When the former set of system parameter combination was applied, the mean error and mean variance are about 0.23 mg/dL and 0.12 mg/dL respectively. With the latter set of system parameters, the mean error and mean variance are 0.24 mg/dL and 0.30 mg/dL respectively.

Table 17. Ethanol Concentration Estimation Using a Common Fitting Parameter Value for Amplitude and Phase with the System Parameter Combination of R = 0.98, dP = 179.62°

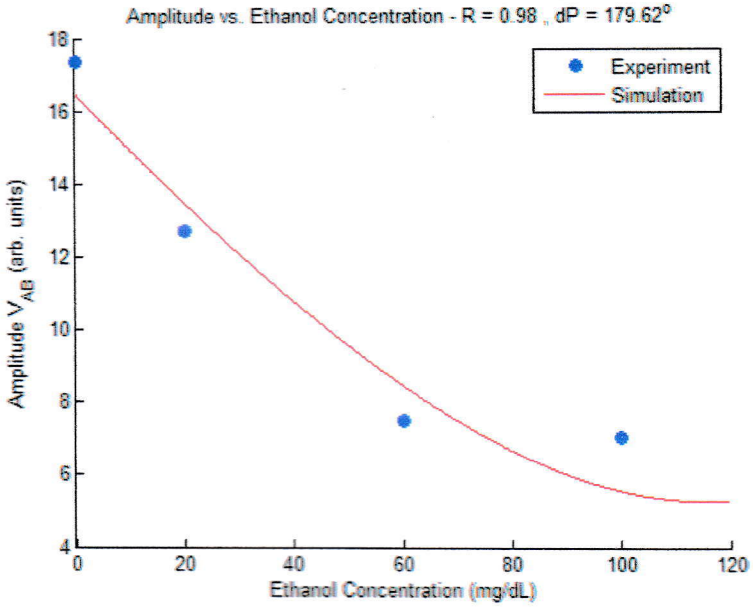
Actual Ethanol Concentration (mg/dL)	Estimated Ethanol Concentration (mg/dL)	Accuracy (Systematic Error in mg/dL)	Precision (Standard Deviation in mg/dL)
0	0.00	0.00	0.00
20	20.66	0.66	0.59
60	60.26	0.26	0.84
100	99.97	0.03	0.39

Table 18. Ethanol Concentration Estimation Using a Common Fitting Parameter Value for Amplitude and Phase with the System Parameter Combination of R = 0.99, dP = 179.68°

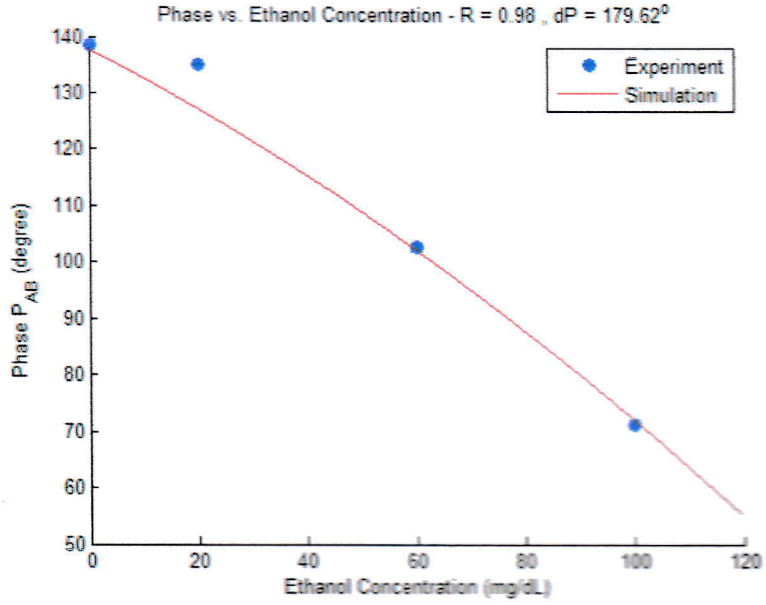
Actual Ethanol Concentration (mg/dL)	Estimated Ethanol Concentration (mg/dL)	Accuracy (Systematic Error in mg/dL)	Precision (Standard Deviation in mg/dL)
0	0.00	0.00	0.00
20	19.36	0.64	0.33
60	59.98	0.02	0.61
100	99.76	0.24	0.06

6.3 Calibration and Evaluation with Different $\bar{\mu}_{IR}$ for Amplitude and Phase

In this approach, $\bar{\mu}_{IR}$ values from 1 to 1000 were swept and optimized separately for amplitude and phase. Unlike the previous approach, for each $\bar{\mu}_{IR}$ value, MSE between the calibrated curve and the experimental results were calculated separately for amplitude and phase. It was found that the smallest MSE is achieved when the amplitude fitting parameter $\bar{\mu}_{IR}$ is set at 174 cm^{-1} for best amplitude fit and the phase fitting parameter $\bar{\mu}_{IR}$ is set at 129 cm^{-1} for best phase fit. Figure 25 and 2Figure 26 are calibration curves obtained for two sets of system parameter combinations with the ethanol concentration estimation results given in Table 19 and Table 20.

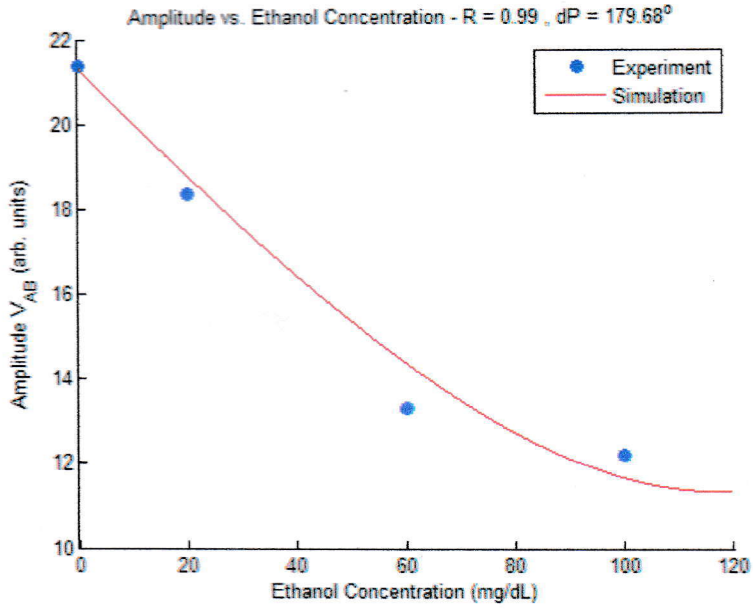


(a)

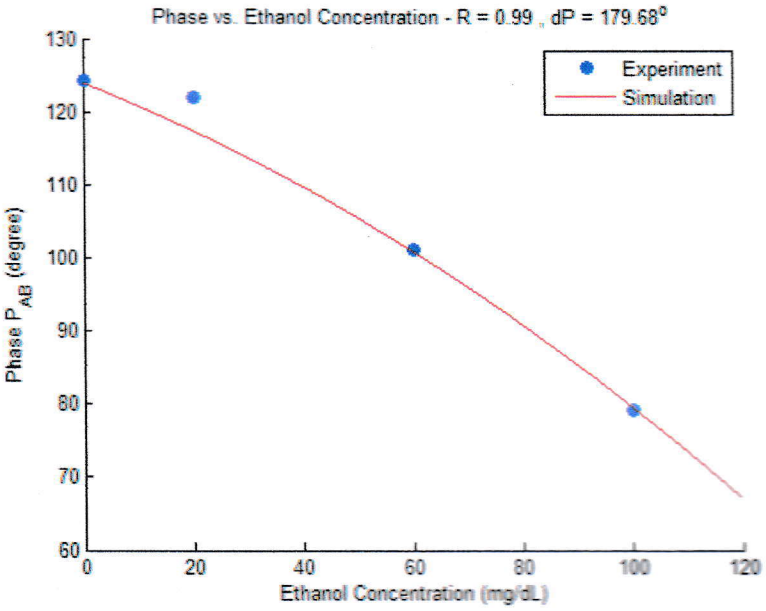


(b)

Figure 25. Ethanol Calibration Curves Using Different Fitting Parameter Values for Amplitude and Phase with the System Parameter Combination of R = 0.98, dP = 179.62°: (a) Differentail Amplitude and (b) Differential Phase



(a)



(b)

Figure 26. Ethanol Calibration Curves Using Different Fitting Parameter Values for Amplitude and Phase with the System Parameter Combination of R = 0.99, dP = 179.68°: (a) Differential Amplitude and (b) Differential Phase

Again, ethanol concentration estimation using WM-DPTR system parameters (R = 0.99, dP = 179.68°) yields better results than with (R = 0.98, dP = 179.62°). When the former set of system parameters were applied, the mean error and mean variance are 0.19 mg/dL and 0.12 mg/dL, respectively. With the latter set of system parameters, the mean error and mean variance are 0.20 mg/dL and 0.32 mg/dL respectively.

Table 19. Ethanol Concentration Estimation Using Different Fitting Parameter Values for Amplitude and Phase with the System Parameter Combination of R = 0.98, dP = 179.62°

Actual Ethanol Concentration (mg/dL)	Estimated Ethanol Concentration (mg/dL)	Accuracy (Systematic Error in mg/dL)	Precision (Standard Deviation in mg/dL)
0	0.00	0.00	0.00
20	20.57	0.57	0.56
60	59.91	0.09	0.87
100	100.12	0.12	0.44

Table 20. Ethanol Concentration Estimation Using Different Fitting Parameter Values for Amplitude and Phase with the System Parameter Combination of R = 0.99, dP = 179.68°

Actual Ethanol Concentration (mg/dL)	Estimated Ethanol Concentration (mg/dL)	Accuracy (Systematic Error in mg/dL)	Precision (Standard Deviation in mg/dL)
0	0.00	0.00	0.00
20	19.50	0.50	0.28
60	60.11	0.11	0.63
100	100.13	0.13	0.02

6.4 Comparison with Other Technologies

From Sections 6.2 and 6.3, if the developed biosensor is calibrated using an optimized common fitting parameter, the accuracy and precision the biosensor can achieve are 0.23 mg/dL and 0.25 mg/dL respectively. When calibrating the developed biosensor using the fitting parameter that is optimized separately for amplitude and phase, the accuracy and precision the biosensor can achieve are 0.19 mg/dL and 0.23 mg/dL, respectively. In addition, one can conclude that, for both settings, the developed biosensor can achieve higher performance when the fitting parameter is optimized for amplitude and phase separately.

Table 21 and Table 22 compare the accuracy, precision, and measurement time of the developed alcohol biosensor with already developed alcohol biosensors and DADSS specifications. The developed WM-DPTR-based alcohol biosensor can exceed the DADSS specifications for both accuracy and precision for all measured ethanol concentrations with a longer measurement time. Its accuracy is comparable to other technologies, but its precision can outperform all other technologies for all measured ethanol concentrations if a longer measurement time is applied.

Table 21. Comparison with Other Alcohol Detection Technologies – Systematic Error

		Autoliv [21]	TruTouch [21]	WM-DPTR	DADSS Specifications [21]
Ethanol Concentration	0			0.00	1
	20	0.2		0.50	1
	60			0.11	0.7
	80	0.8	0.1		0.3
	100			0.13	
	120	0.0			1
In-vivo or In-vitro		In-vitro	In-vitro	In-vitro	
Measurement Time		5 sec.	30 sec.	120 sec.	325 ms
Units for systematic error: mg/dL. Shaded areas: Information is not available.					

Table 22. Comparison with Other Alcohol Biosensors – Standard Deviation

		Autoliv [21]	TruTouch [21]	WM-DPTR	DADSS Specifications [21]
Ethanol Concentration	0			0.00	1
	20	1.7		0.28	1
	60			0.63	0.7
	80	2.2	1.6		0.3
	100			0.02	
	120	2.7			0.1
In-vivo or In-vitro		In-vitro	In-vitro	In-vitro	
Measurement Time		5 sec.	30 sec.	120 sec.	325 ms
Units for standard deviation: mg/dL. Shaded areas: Information is not available.					

Chapter 7
Limitations and Future Directions

Although efforts were made to simulate close to alcohol detection in the interstitial fluid of the dermis layer, all measurement results were done on phantoms and thus no in-vivo measurement results were obtained. The ethanol measurements were done using fairly-old lasers. Thus, the laser intensity variations due to temperature changes had negative impacts on the performance of the developed biosensor and longer measurement time had to be applied. In addition, the same alcohol measurement data was used for obtaining the calibration curves and for alcohol biosensor evaluation. Hence, the biosensor evaluation results only show the level performance the developed biosensor can achieve.

The main drawbacks of the current system are its cost and size. However, these can be overcome with new technologies. The system components that drive up the developed alcohol biosensor cost and size are the quantum cascade lasers, which can cost $60 000 [49], function generators, and the lock-in amplifier. With current technologies, the functions generators and the lock-in amplifier can be shrunk into a data acquisition card with the size of a microprocessor and cost of hundreds of dollars [50]. With the increase in laser applications in the MIR range, many research groups attempt to develop a low cost laser for the MIR range. Axel et al. demonstrate the use of a low-noise Yb:fiber frequency comb to produce mW-level MIR pulse trains tunable over a range of 3-10 μm [51]. In addition, Daylight Solutions, a major quantum cascade laser manufacturer, has developed a broadly tunable, quantum cascade laser for 7-13 um range, as shown in Figure 27 [52]. Also, Laser Components, a laser manufacturer, is selling cell-phone-sized pulsed diode lasers, illustrated in Figure 28, for 4.7 μm, 5.5 μm, and 9.5 μm wavelengths [53].

With the above in mind, the potential improvements to the developed alcohol biosensor include:

- Replacing the hardware function generators and lock-in amplifier with a data acquisition cards that can be integrated into a microprocessor

- Replacing the current large laser systems with a smaller and broadly tunable one so that the laser can switch between 9.5 um and 10.4 um and one laser is needed or with two small MIR diode lasers

Future directions include shrinking and reducing the cost of the system, biosensor calibration and evaluation using measurement data from different dates, fine-tuning the system for better alcohol detection in 0-100 mg/dL ethanol concentration range, and performing clinical trials.

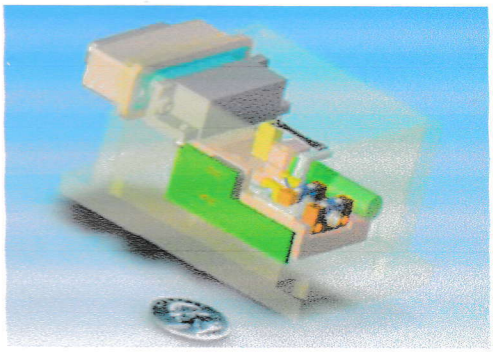


Figure 27. New Quantum Cascade Laser Diagram [51]

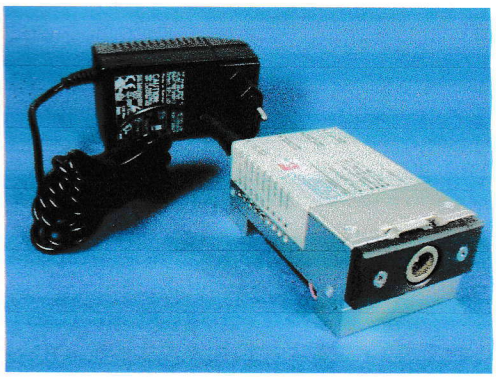


Figure 28. Cell-Phone-Sized Pulsed Diode MIR Lasers Diode [53]

Chapter 8
Significance and Conclusion

8.1 Conclusion and Thesis Novel Contributions

In this thesis, a WM-DPTR-based alcohol biosensor is developed. During the process, many novel contributions were made. A fifth type of alcohol detection technologies, based on differential photothermal radiometry, is introduced. Although the concept has been applied to glucose measurements, it was not, to the best of the author's knowledge, applied to alcohol detection applications.

The developed alcohol sensor differs from other alcohol detection technologies in a number of aspects especially in that:

- a multi-channel approach was used
- two out-of-phase laser beams were used to perform differential measurements
- ethanol measurements depend on both changes in thermal and optical properties instead on only thermal or optical properties
- the system can be sensitively-tuned to achieve high performance results for a certain range of ethanol concentration

The research was carried out in three phases. In the first phase, ethanol measurements were performed using three different phantoms: ethanol and water solutions, ethanol and serum solutions, and ethanol and serum solutions diffused through skin. By comparing experimental results to simulation results, one can observe that the simulation and experimental results are well in-line with each other, confirming the validity of both the experimental results and the mathematic model of WM-DPTR system. Also, a piecewise analytical approach were used to highlight the sensitivity tunability property of the system. The high sensitivity of the developed alcohol biosensor demonstrates the feasibility in ethanol measurement in the 0-100 mg/dL ethanol concentration range.

Also, in the second phase, using the developed ethanol simulator, calibration curves were obtained by optimizing the fitting parameters to achieve the best fit between the calibration curves and ethanol measurement results. This was done using two approaches: optimizing for a single fitting parameter value for both amplitude and phase and optimizing for two different fitting parameters for amplitude and phase.

Finally, the WM-DPTR-based alcohol biosensor was evaluated using the calibration curves and ethanol measurement results. From the analysis of the experimental data, the developed biosensor exhibits high sensitivity and linearity. The best ethanol concentration estimation results, in terms of accuracy and precision, are obtained when the best-fits of the experimental data to WM-DPTR theory are done separately for amplitude and phase, resulting in better fitting between calibration curves and experimental results. Using that calibration approach, the calibrated biosensor can achieve a very-good-to-excellent accuracy of 0.19 mg/dL in mean error in the case of ethanol and human serum solutions diffused through skin, which is comparable to state-of-the-art commercial non-invasive ethanol sensors. Furthermore, it outperforms other alcohol detection technologies in terms of precision, realizing a high precision of 0.12 mg/dL in mean variance, with a longer measurement time. However, it is expected that the ethanol measurement time using the WM-DPTR-based biosensor will decrease substantially with state-of-the-art quantum cascade lasers.

8.2 Significance

The developed new non-invasive BAC biosensor for in-vehicle use can radically change state-of-the-art ignition interlock technologies and improve their performance to prevent impaired driving. It was demonstrated that this new in-vehicle alcohol biosensor can achieve high sensitivity, accuracy, precision, and linearity by taking advantage of the properties of the WM-DPTR technique.

The technical challenges in developing a good BAC biosensor are substantial, however the possible benefits to society are compelling, with the potential to prevent about 63 821 motor vehicle injuries and 210 932 vehicles damaged and to save approximately $20.62 billion every

year if all drivers with BACs at or above the legal limit (80 mg/dL) are compelled not to drive under the influence of alcohol [54].

Although this thesis focuses on the use of the developed biosensor in ignition interlocks, the developed alcohol biosensor can be used in other applications. One application is alcohol monitoring system. Alcohol misuse can lead to multiple side-effects resulting in physical and mental harm, accidents, assaults, fights, and other traumatic events requiring hospital care. In fact, according to a study, about 2–40% of all emergency department attendances are due to alcohol-related problems. In such cases, having an alcohol monitoring system can help medical staffs better assess the patient's situation, manage the patient's health problems, and determine the best treatment for the patient [55, 56].

Another application of alcohol biosensor is to incorporate them into personal testers that are used to manage the user's consumption level, prevent him or her from alcohol misuse, and protect him or her from alcohol side-effects [57].

References

[1] Boggan, W. (2003). *Understanding Alcohol: Investigations into Biology and Behavior*. Colorado Springs, CO: BSCS.

[2] Canadian Alcohol and Drug Use Monitoring Survey. (2014, February 4). Retrieved January 15, 2015, from http://www.hc-sc.gc.ca/hc-ps/drugs-drogues/stat/_2011/summary-sommaire-eng.php#share

[3] Zakhari, S. (2006). Overview: how is alcohol metabolized by the body?. *Alcohol Research & Health*.

[4] Overview - Blood Alcohol Concentration (BAC). (2014, July). Retrieved January 15, 2015, from http://www.madd.ca/madd2/en/impaired_driving/impaired_driving_bac.html

[5] Perreault, S. (2013). Impaired driving in Canada, 2011. *Juristat*. Statistics Canada Catalogue no. 85-002-X.

[6] Drinking and Driving Facts. *Answering All Your DUI Questions*. Retrieved November 10, 2013, from http://duicanadainfo.com/drinking-and-driving-facts.php

[7] Alcohol-impaired driving. *Fatality Facts*. Retrieved November 10, 2013, from http://www.iihs.org/iihs/topics/t/alcohol-impaired-driving/fatalityfacts/alcohol-impaired-driving

[8] Impaired Driving in Canada. *Drunk Driving in Canada Finding an Impaired Driving Lawyer*. Retrieved November 10, 2013, from http://www.dui.ca/

[9] Willis, C., Lybrand, S., & Bellamy, N. (2004). Alcohol ignition interlock programmes for reducing drink driving recidivism. *Cochrane Database Syst Rev*, *4*.

[10] Impaired Driving. (2013, September 11). *Ignition Interlock*. Retrieved November 10, 2013, from http://www.mto.gov.on.ca/english/safety/impaired/interlock.shtml

[11] Beitel, G. A., Sharp, M. C., & Glauz, W. D. (2000). Probability of arrest while driving under the influence of alcohol. *Injury Prevention, 6*(2), 158-161.

[12] Interlock Facts. *Interlocks in all cars*. Retrieved November 10, 2013, from http://interlockfacts.com/interlocks-in-all-cars/

[13] Ferguson, S. A., Traube, E., Zaouk, A., & Strassburger, R. (2009). Driver Alcohol Detection System for Safety (DADSS) - A Non-Regulatory Approach in the Development and Deployment of Vehicle Safety Technology to Reduce Drunk Driving. In *Proceedings Of The 21st (Esv) International Technical Conference On The Enhanced Safety Of Vehicles,* (Stuttgart, Germany)

[14] Ferguson, S., and Traube, E. (2010, April) Using Technology to Eliminate Drunk Driving. *NHTSA*. Retrieved November 12, 2013, from http://www.nhtsa.gov/DOT/NHTSA/NVS/Public%20Meetings/Presentations/2010%20Meetings/HyundaiDADSS.pdf

[15] Guo, X., Mandelis, A., &Zinman, B. (2012). Noninvasive glucose detection in human skin using wavelength modulated differential laser photothermal radiometry. *Biomedical optics express, 3*(11), 3012-3021

[16] Doroshenko, I., Pogorelov, V., & Sablinskas, V. (2012). Infrared absorption spectra of monohydric alcohols. *Dataset Papers in Science*.

[17] X. Guo, A. Mandelis, A. Matvienko, K. Sivagurunathan, and B. Zinman. (2010, July 27 – 30). Wavelength-modulated differential photothermal radiometry for non-Invasive blood glucose detection. *In Proc. 10th Int. Conf. on Quantitative InfraRed Thermography*. Abstract presented at the QIRT10 Quebec (p.12). Quebec City, Canada: Conference.

[18] Venugopal M et al. (2008). Clinical evaluation of a novel interstitial fluid sensor system for remote continuous alcohol monitoring.*Sensors Journal, IEEE, 8*(1), 71-80.

[19] Guo, X., Mandelis, A., Liu, Y., Chen, B., Zhou, Q., & Comeau, F. (2014). Noninvasive In-Vehicle Alcohol Detection with Wavelength-Modulated Differential Photothermal Radiometry. *Biomed. Opt. Express, 5 (7),* 2333-2340.

[20] Ridder, T. D., Ver Steeg, B. J., Vanslyke, S. J., & Way, J. F. (2009, February). Noninvasive NIR Monitoring of Interstitial Ethanol Concentration. In *SPIE BiOS: Biomedical Optics,* 71860E-1-71860E-11.

[21] Ferguson, S. A., Zaouk, A., Dalal, N., Strohl, C., Traube, E., and Strassburger, R. (2011, June). Driver Alcohol Detection System for safety (DADSS) — Phase I Prototype Testing and Findings. *22nd International Technical Conference on the Enhanced Safety of Vehicles.*

[22] Hök, B., Pettersson, H., & Andersson, G. (2006, May). Contactless measurement of breath alcohol. In *Proc. Micro Structure Workshop.*

[23] Win, D. T. (2006). Breath Alcohol Testers-Prevents Road Accidents. *Assumption Univ J Technol, 10,* 75-80.

[24] Hsieh, T. (2012, December 15). Alcosensors - Fuel Cell Alcohol Detectors. *BIOE 414 Instrumentation Projects*. Retrieved June 25, 2014, from https://wiki.engr.illinois.edu/display/BIOE414/Alcosensors+Fuel+Cell+Alcohol+Detectors

[25] American Beverage Institute. *Alcohol Detection Technologies: Present and Future.* Berman and Company, Washington DC., 2009.

[26] ALERT™ J5. *ACS Corporation*. Retrieved June 25, 2014, from http://acs-corp.com/products/law-enforcement/alert-j5/

[27] Marques, P. & McKnight, A. (2007). Evaluating Transdermal Alcohol Measuring Devices. *National Highway Traffic Safety Administration.*

[28] Dai, J., Teng, J., Bai, X., Shen, Z., & Xuan, D. (2010, March). Mobile phone based drunk driving detection. In *Pervasive Computing Technologies for Healthcare, 2010 4th IEEE International Conference on,* 1-8.

[29] *The Visual Detection of DWI Motorists*. (1998). Washington, D.C.: U.S. Dept. of Transportation, National Highway Traffic Safety Administration.

[30] Pollard, J. K., Nadler, E. D., & Stearns, M. D. (2007). Review of Technology to Prevent Alcohol Impaired Crashes (TOPIC). In *U.S. Department of Transportation, National Highway Traffic Safety Administration.*

[31] Mandelis, A., & Guo, X. (2011). Wavelength-modulated differential photothermal radiometry: theory and experimental applications to glucose detection in water. *Physical Review E, 84*(4), 041917-1-041917-14.

[32] Almond, D., & Patel, P. (1996). *Photothermal science and techniques*. London: Chapman & Hall.

[33] Mandelis, A. (1994). Signal-to-noise ratio in lock-in amplifier synchronous detection: A generalized communications systems approach with applications to frequency, time, and hybrid (rate window) photothermal measurements. *Review of scientific instruments, 65*(11), 3309-3323.

[34] Mandelis, A. (2001). *Diffusion-Wave Fields Mathematical Methods and Green Functions*. New York, NY: Springer New York.

[35] Mandelis, A., & Guo, X (2014, February). Method Of Performing Wavelength Modulated Differential Laser Photothermal Radiometry With High Sensitivity. *U.S. Patent No. 8649835*. Washington, DC: U.S. Patent and Trademark Office.

[36] Jacques, S. L. (2013). Optical properties of biological tissues: a review.*Physics in medicine and biology*, *58*(11), R37.

[37] Richter, C., Viljoen, H. J., & Van Rensburg, N. F. J. (2003). Effective thermal conductivity estimates of particulate mixtures. *Journal of applied physics*,*93*(5), 2663-2670.

[38] Matvienko, A., & Mandelis, A. (2005). High-precision and high-resolution measurements of thermal diffusivity and infrared emissivity of water–methanol mixtures using a pyroelectric thermal wave resonator cavity: frequency-scan approach. *International Journal of Thermophysics*, *26*(3), 837-854.

[39] Bashkatov, A. N., Genina, E. A., & Tuchin, V. V. (2011). Optical properties of skin, subcutaneous, and muscle tissues: a review. *Journal of Innovative Optical Health Sciences*, *4*(01), 9-38.

[40] Stein, S. (2005, June). Infrared Spectra. In *NIST Chemistry WebBook, NIST Standard Reference Database Number 69, Eds. P.J. Linstrom and W.G. Mallard*. Gaithersburg MD, 20899: National Institute of Standards and Technology, http://webbook.nist.gov, (retrieved January 19, 2015).

[41] Wieliczka, D. M., Weng, S., & Querry, M. R. (1989). Wedge shaped cell for highly absorbent liquids: infrared optical constants of water. *Applied Optics*, *28*(9), 1714-1719.

[42] Wang, J., & Fiebig, M. (1995). Measurement of the thermal diffusivity of aqueous solutions of alcohols by a laser-induced thermal grating technique. *International journal of thermophysics*, *16*(6), 1353-1361.

[43] Dai, T., Pikkula, B. M., Wang, L. V., & Anvari, B. (2004). Comparison of human skin opto-thermal response to near-infrared and visible laser irradiations: a theoretical investigation. *Physics in medicine and biology*, *49*(21), 4861-4877

[44] Michel, A. P., Liakat, S., Bors, K., & Gmachl, C. F. (2013). In vivo measurement of mid-infrared light scattering from human skin. *Biomedical optics express*, *4*(4), 520-530.

[45] Hasgall, P., Neufeld, E., & Gosselin, M. (2013). IT'IS Database for thermal and electromagnetic parameters of biological tissues. Version 2.6, January 13th, 2015.

[46] Giovenale, E., D'Arienzo, M., Doria, A., Gallerano, G. P., Lai, A., Messina, G., & Piccinelli, D. (2003). Absorption and diffusion measurements of biological samples using a THz free electron laser. *Journal of biological physics*, *29*(2), 159-170.

[47] SR850 - Lock In Amplifier. Retrieved January 26, 2015, from http://www.thinksrs.com/products/SR850.htm

[48] Alpat, Ş., & Telefoncu, A. (2010). Development of an alcohol dehydrogenase biosensor for ethanol determination with toluidine blue O covalently attached to a cellulose acetate modified electrode. *Sensors*, *10*(1), 748-764.

[49] Hungry for Your MIR Thoughts. (2015). Retrieved January 26, 2015, from https://www.thorlabs.com/NewGroupPage9.cfm?ObjectGroup_ID=1858

[50] TPCX Data Acquisition Card. (2014). Retrieved January 26, 2015, from http://www.elsys-instruments.com/products/tpcx.php

[51] Ruehl, A., Gambetta, A., Hartl, I., Fermann, M. E., Eikema, K. S., & Marangoni, M. (2012). Widely-tunable mid-infrared frequency comb source based on difference frequency generation. Optics letters, 37(12), 2232-2234.

[52] Weida, M. J., & Yee, B. (2011, February). Quantum cascade laser-based replacement for FTIR microscopy. In *SPIE BiOS*. International Society for Optics and Photonics.

[53] Pulsed Laser Diodes in the Mid-IR. (2011, September 6). Retrieved May 3, 2015, from http://www.lasercomponents.com/uk/news/pulsed-laser-diodes-in-the-mid-ir-5/

[54] Overview - Statistics. *MADD Canada*. Retrieved November 10, 2013, from http://madd.ca/madd2/en/impaired_driving/impaired_driving_statistics.html

[55] Alcohol's Effects on the Body. *National Institute on Alcohol Abuse and Alcoholism (NIAAA)*. Retrieved August 2, 2014, from http://www.niaaa.nih.gov/alcohol-health/alcohols-effects-body

[56] Charalambous, M. P. (2002). Alcohol and the Accident and Emergency Department: a Current Review. *Alcohol and alcoholism*, *37*(4), 307-312.

[57] Underage Drinking Prevention - Teen Alcohol Testing - Concerned Parents. Retrieved January 26, 2015, from http://www.lifeguardbreathtester.com/Popular_Uses/family.shtml

Appendix: Manuscript of First Author Publication

Absolute calibration method of ethyl alcohol biosensor based on wavelength-modulated differential photothermal radiometry

Yi Jun Liu[1,2], Andreas Mandelis[1,2,*], and Xinxin Guo[1]

[1] *Center for Advanced Diffusion-Wave Technologies (CADIFT), Department of Mechanical and Industrial Engineering, University of Toronto, Toronto, M5S 3G8, Canada*

[2] *Institute of Biomaterials and Biomedical Engineering, University of Toronto, Toronto, M5S 3G9*

[*] mandelis@mie.utoronto.ca

Abstract: In this work, laser-based wavelength-modulated differential photothermal radiometry (WM-DPTR) is applied to develop a non-invasive in-vehicle alcohol biosensor. WM-DPTR features unprecedented ethanol-specificity and sensitivity by suppressing baseline variations through a differential measurement near the peak and baseline of the mid-infrared ethanol absorption spectrum. Biosensor signal calibration curves are obtained from WM-DPTR theory and from measurements in human blood serum and ethanol solutions diffused from skin. The results demonstrate that the WM-DPTR-based calibrated alcohol biosensor can achieve high precision and accuracy for the ethanol concentration range of 0–100 mg/dL. The high-performance alcohol biosensor can be incorporated in ignition interlocks that could be fitted as a universal accessory in vehicles in efforts to reduce incidents of drinking and driving.

©2015 Optical Society of America

OCIS codes: (280.1415) Biological sensing and sensors; (170.1470) Blood or tissue constituent monitoring; (300.6430) Spectroscopy, photothermal

References and links

1. S. Perreault, "Impaired driving in Canada, 2011", Statistics Canada—Catalogue no. 85-002-X, (2013).
2. Impaired Driving in Canada, "Drunk Driving in Canada Finding an Impaired Driving Lawyer," http://www.dui.ca.
3. C. Willis, S. Lybrand, and N. Bellamy, "Alcohol ignition interlock programmes for reducing drink driving recidivism," Cochrane Database Syst. Rev. **18**(4), CD004168 (2004).
4. G. A. Beitel, M. C. Sharp, and W. D. Glauz, "Probability of arrest while driving under the influence of alcohol," Injury Prevention **6**(2), 158-161 (2000).
5. Interlock Facts, "Interlocks in all cars," http://interlockfacts.com/interlocks-in-all-cars.
6. S. A. Ferguson and E. Traube, "Using Technology to Eliminate Drunk Driving," http://www.nhtsa.gov/DOT/NHTSA/NVS/Public%20Meetings/Presentations/2010%20Meetings/HyundaiDADSS.pdf.
7. S. A. Ferguson, E. Traube, A. Zaouk, and R. Strassburger, "Driver alcohol detection system for safety (DADSS) – a non-regulatory approach in the development and deployment of vehicle safety technology to reduce alcohol impaired driving", in Proceedings of the 21st International Technical Conference on the Enhanced Safety of Vehicles, (Stuttgart, Germany, 2009), pp. 09–0464.
8. T. D. Ridder, B. J. Ver Steeg, S. J.Vanslyke, and J. F. Way, "Noninvasive NIR Monitoring of Interstitial Ethanol Concentration," Proc. SPIE **7186**, 71860E (2009).
9. S. A. Ferguson, A. Zaouk, N. Dalal, C. Strohl, E. Traube, and R. Strassburger, "Driver alcohol detection system for safety (DADSS) – phase 1 prototype testing and findings", in Proceedings of the 22rd International Technical Conference on the Enhanced Safety of Vehicles, (Washington, D.C., US, 2011), pp. 11–0230.
10. M. Venugopal, K. E. Feuvrel, D. Mongin, S. Bambot, M. Faupel, A. Panangadan, A. Talukder, and R. Pidva, "Clinical evaluation of a novel interstitial fluid sensor system for remote continuous alcohol monitoring," IEEE Sensors J. **8**(1), 71–80 (2008).
11. B. Hök, H. Pettersson, and G. Andersson, "Contactless measurement of breath alcohol," in Proceedings of Micro Structure Workshop, (Västerås, Sweden, 2006), pp.36-Ble
12. A. Mandelis and X. Guo, "Method of performing wavelength modulated differential laser photothermal radiometry with high sensitivity," US Patent No. 08649835 Cl. 600–316, issued on Feb. 11, 2014.

13. X. Guo, A. Mandelis, Y. Liu, B. Chen, Q. Zhou, and F. Comeau, "Noninvasive In-Vehicle Alcohol Detection with Wavelength-Modulated Differential Photothermal Radiometry," Biomedical Optics Express **5** (7), 2333-2340 (2014).
14. I. Doroshenko, V. Pogorelov, and V. Sablinskas, "Infrared absorption spectra of monohydric alcohols," Dataset Papers in Chemistry **2013**, 329406 (2013).
15. A. Mandelis and X. Guo, "Wavelength-modulated differential photothermal radiometry: theory and experimental applications to glucose detection in water," Phys. Rev. E. **84**(4), 041917 (2011).
16. S. L. Jacques, "Optical properties of biological tissues: a review," Physics in Medicine and Biology **58**(11), R37 (2013).
17. C. Richter, H. J. Viljoen, and N. F. J. V. Rensburg, "Effective thermal conductivity estimates of particulate mixtures," Journal of Applied Physics **93**(5), 2663-2670 (2003).
18. A. Matvienko and A. Mandelis, "High-precision and high-resolution measurements of thermal diffusivity and infrared emissivity of water–methanol mixtures using a pyroelectric thermal wave resonator cavity: frequency-scan approach," International Journal of Thermophysics **26**(3), 837-854 (2005).
19. A. N. Bashkatov, E. A. Genina, and V. V. Tuchin, "Optical properties of skin, subcutaneous, and muscle tissues: a review," Journal of Innovative Optical Health Sciences **4**(1), 9-38 (2011).
20. NIST Mass Spec Data Center, S.E. Stein, director, "Infrared Spectra," in *NIST Chemistry WebBook, NIST Standard Reference Database Number 69*, P.J. Linstrom and W.G. Mallard, eds. (National Institute of Standards and Technology, 2003), http://webbook.nist.gov.
21. D. M. Wieliczka, S. Weng, and M. R. Querry, "Wedge shaped cell for highly absorbent liquids: infrared optical constants of water," Applied Optics **28**(9), 1714-1719 (1989).
22. J. Wang and M. Fiebig, "Measurement of the thermal diffusivity of aqueous solutions of alcohols by a laser-induced thermal grating technique," International Journal of Thermophysics **16**(6), 1353-1361 (1995).
23. T. Dai, B. M. Pikkula, L. V. Wang, and B. Anvari, "Comparison of human skin opto-thermal response to near-infrared and visible laser irradiations: a theoretical investigation," Physics in Medicine and Biology **49**(21), 4861-4877 (2004).
24. A. P. Michel, S. Liakat, K. Bors, and C. F. Gmachl, "In vivo measurement of mid-infrared light scattering from human skin," Biomedical Optics Express **4**(4), 520-530 (2013).
25. P. A. Hasgall, E. Neufeld, M. Gosselin, A. Klingenbock, and N. Kuster, "IT'IS Database for thermal and electromagnetic parameters of biological tissues, Version 2.6," (IT'IS Foundation, 2015), http://www.itis.ethz.ch/database.
26. E. Giovenale, M. D'Arienzo, A. Doria, G. P. Gallerano, A. Lai, G. Messina, and D. Piccinelli, "Absorption and diffusion measurements of biological samples using a THz free electron laser," Journal of Biological Physics **29**(2), 159-170 (2003).

1. Introduction

In Canada, alcohol-impaired driving is the leading cause of criminal deaths [1]. Police in 2011 reported 90,277 impaired driving incidents in which the drivers' blood alcohol concentration (BAC) was over the legal limit of 0.08 g/dL, which is about 3,000 more incidents than in 2010 [1,2]. While current countermeasures such as fines, incarceration, license revocations and vehicle impoundments are ineffective in preventing drunk driving because they do not modify violators' driving habits, studies have indicated that ignition interlock devices (IIDs) which may be installed in the vehicles of those convicted of driving while intoxicated (DWI) can reduce recidivism by about two thirds. However, the probability of arrest while driving with BAC over the legal limit is about one in 200 [3,4]. To overcome this drawback, Mothers Against Drunk Driving (MADD) has called for ignition interlocks to become standard equipment in all motor vehicles sold [5]. Current IIDs are sensitive to changes in the environment, use significant energy for heating, take a long time to perform a measurement, exhibit some drift in response, and require very frequent maintenance and calibration services. In addition, they require the driver to deliver a delicate breath into the device before starting the vehicle and run random retests during driving, thereby distracting the driver from the driving task [6].

An effort is underway to develop alcohol detection technologies that could be fitted in vehicles and should be non-invasive, reliable, durable, quick to use, seamless with the driving task and require little or no maintenance [7]. Alcohol detection technologies can be grouped into one of four technology types: (1) tissue spectrometry that estimates BAC from a near-infrared (NIR) beam diffusely reflected from the interstitial fluid (ISF) in the dermis of the subject's skin [8]; (2) distant spectrometry that analyzes BAC by using measurements of exhaled carbon dioxide (CO_2) based on mid-infrared (MIR) spectroscopy as an indication of

the degree of dilution of the alcohol in exhaled air; (3) fuel-cell based electrochemical devices in which BAC is determined from the current produced by the oxidation of ethanol; and (4) a behavioral system that attempts to identify cues of typical drunk driving behavior related to lane position maintenance, speed control, judgment, and vigilance [9].

Out of these four technology categories, the Driver Alcohol Detection System for Safety (DADSS) has chosen only tissue-spectrometry-based TruTouch and distant-spectrometry-based Autoliv technologies for prototype development. TruTouch, operating in the NIR range of 1.25 – 2.5 μm, transmits light into the skin in contact with an optical touchpad and collects and analyzes the diffusely reflected light to determine the subject's BAC [10]. However, TruTouch's selectivity is limited by weak ethanol absorption in NIR and confounding absorptions from other skin tissue components, such as skin pigments, to which NIR tissue spectroscopy is sensitive. The Autoliv system draws cabin air from the car into its optical module through a breathing cup which is subsequently analyzed by a detector to determine the external concentration of ethanol and CO_2. The approach assumes that alveolar CO_2 concentration remains constant. However, in practice, alveolar CO_2 concentration varies from person to person and with the level of physical activity [11], which complicates the calibration procedure and introduces false readings.

In comparison, WM-DPTR, a non-invasive, non-contacting, and patented [12] mid-infrared thermophotonic technique for measuring low concentrations of solutes in strongly absorbing fluids like water and blood, presents itself as a very promising technology for alcohol detection and can overcome the above-mentioned difficulties. Its unique photothermal properties enable it to overcome the shallow MIR optical penetration depth due to high water absorption and allow for signal amplification due to combined optical and thermal changes of the ISF with BAC. Our previous work [13] has demonstrated the potential and feasibility of WM-DPTR method for ethyl alcohol detection. In this paper, a calibration method is developed for the WM-DTPR-based alcohol biosensor using a combined theoretical and experimental approach with ethanol and human serum solutions diffused from skin to convert the device into an accurate and precise alcohol detector.

2. Methods

2.1 WM-DPTR Experimental Setup

The WM-DPTR system [12] consists of two quantum cascade lasers (QCL) emitting at the peak (9.5 μm or 1042 cm^{-1}) and at the baseline (10.4 μm or 962 cm^{-1}) of the ethanol mid-infrared absorption band, as illustrated in Fig. 1. The experimental system is shown in Fig. 2. Two function generators produce a phase-locked square wave to modulate the laser beams and control the phase difference *dP* between the beams. The laser modulation frequency which controls the probing depth is set at 90 Hz to generate a probe depth < 40 μm in the epidermis layer and below the stratum corneum to achieve ethyl alcohol detection in the ISF. A motorized variable circular mid-IR neutral density (ND) filter (Reynard Corp, CA) is placed in front of laser B and controls the intensity ratio $R = I_A / I_B$ of the two lasers. The differential photothermal radiometry (DPTR) infrared (thermal) photon signal generated by the two out-of-phase square-wave-modulated laser beams irradiating the sample is collected by a pair of parabolic mirrors and focused onto a HgCdZnTe detector with high detectivity in the 2-5 μm spectral range. The output from the MCZT detector is then sent to a lock-in amplifier for demodulation and analysis. Using LabView software, the system includes feedback for controlling the phase difference dP and the power ratio R of the two lasers, henceforth referred to as "the system parameters", through rotational adjustment of the neutral density filter and temporal adjustment of the two square-wave modulation waveforms. Experimental results with the WM-DPTR-based ethanol biosensor [13] used for developing the present calibration purposes are shown in Fig. 3. For the given system parameter combination of (R = 0.99, dP = 179.68), as the ethanol concentration increases from 0 mg/dL to 100 mg/dL, the differential amplitude V_{AB} decreases by about 43% and the differential phase P_{AB} by about

36%. Thus, WM-DPTR measurements of ethanol concentrations in the 0-100 mg/dL range are well-resolved for both amplitude and phase.

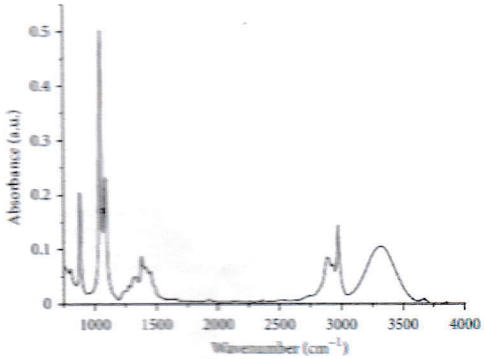


Fig. 1. Mid-Infrared Optical Absorption Spectrum of Liquid Ethanol [14]

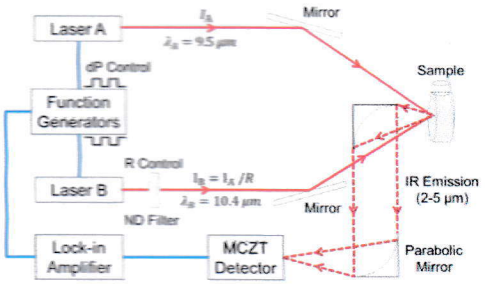


Fig. 2. WM-DPTR System Configuration

2.2 WM-DPTR Theory

It has been shown [15] that the DPTR signal generated by each laser is given by:

$$\Delta Q_j(t) = \frac{I_o \alpha \mu_{ej} \bar{\mu}_{IR}}{2k} K(\lambda_1,\lambda_2)\tau_{tj} \left\{ \begin{array}{l} \dfrac{1}{\bar{\mu}_{IR}+\mu_{ej}}\left[W\left(\sqrt{\dfrac{t}{\tau_{tj}}}\right) + W\left(\sqrt{\dfrac{t}{\tau_{IR}}}\right) - 2 \right] \\ + \dfrac{1}{\bar{\mu}_{IR}-\mu_{ej}}\left[W\left(\sqrt{\dfrac{t}{\tau_{tj}}}\right) - W\left(\sqrt{\dfrac{t}{\tau_{IR}}}\right) \right] \\ + \dfrac{2}{\bar{\mu}_{IR}}\left\{ 2\sqrt{\dfrac{t}{\pi\tau_{tj}}} - \sqrt{\dfrac{\tau_{IR}}{\tau_{tj}}}\left[1 - W\left(\sqrt{\dfrac{t}{\tau_{IR}}}\right) \right] \right\} \end{array} \right\} \quad (1)$$

where j = A, B with ΔQ_A (t) and ΔQ_B (t) being the DPTR signal generated by laser A and laser B respectively, I_o is the laser intensity, α is the thermal diffusivity of the sample, μ_e is its absorption coefficient, $\bar{\mu}_{IR}$ is its spectrally weighted IR emission coefficient, k is its thermal conductivity, $K(\lambda_1,\lambda_2)$ is a factor related to IR detector bandwidth defined by $[\lambda_1,\lambda_2]$, $\tau_t = (\mu_e^2\alpha)^{-1}$ and $\tau_{IR} = (\bar{\mu}_{IR}^2\alpha)^{-1}$ are photothermal time constants, and $W(x) = e^{x^2}\, erfc(x)$ with erfc(x) being the complementary error function. In practice, $\bar{\mu}_{IR}$ is a fitting parameter to experimental data.

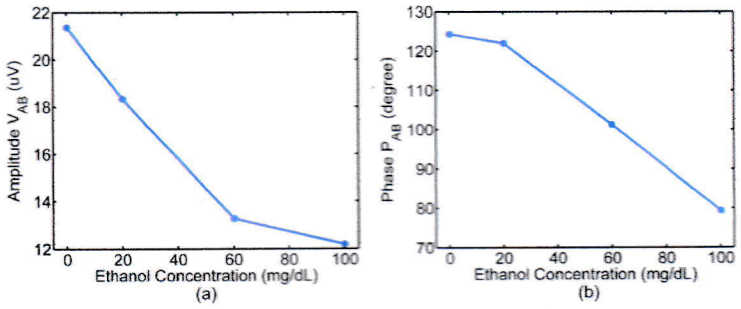


Fig. 3. WM-DPTR-Based Alcohol Biosensor Measurement Results – Ethanol and Human Serum Solutions Diffused through Skin

For the WM-DPTR measurements, only laser A is turned on during $0 \le t \le \tau_p$ while only laser B is turned on during $\tau_p \le t \le \tau_o$ with τ_o being the repetition period of the modulated pulse and $\tau_p = \tau_o / 2$. For the full period $0 \le t \le \tau_o$, the sequence of photothermal responses can be described as:

$$S_{AB}(t) = \begin{cases} \Delta Q_A(t)u(t) - \Delta Q_A(t-\tau_p)u(t-\tau_p) \\ +\Delta Q_B(t-\tau_p)u(t-\tau_p) + \Delta Q_B(t+\tau_p) - \Delta Q_B(t) \end{cases}; 0 \le t \le \tau_o \quad (2)$$

where u(t) is the unit step or Heaviside function.

In most cases, the transient decays are slow and occur over N periods. Thus, S_{AB} should include contributions from earlier decaying transients from lasers A and B from prior N periods. The complete set of signal contributions from photothermal transients of earlier periods is:

$$S_{AB0}(t) = \begin{cases} \Delta Q_A(t)u(t) - \Delta Q_A(t-\tau_p)u(t-\tau_p) \\ +\Delta Q_B(t-\tau_p)u(t-\tau_p) \end{cases}; 0 \le t \le \tau_o$$

$$S_{AB-1}(t) = \begin{cases} \Delta Q_A(t+\tau_0)u(t+\tau_0) - \Delta Q_A(t+\tau_p)u(t+\tau_p) \\ +\Delta Q_B(t+\tau_p)u(t+\tau_p) - \Delta Q_B(t)u(t) \end{cases}; -\tau_o \le t \le 0$$

$$\vdots$$

$$S_{AB-N}(t) = \begin{cases} \Delta Q_A(t+N\tau_o)u(t+N\tau_o) \\ -\Delta Q_A(t+N\tau_o-\tau_p)u(t+N\tau_o-\tau_p) \\ +\Delta Q_B(t+N\tau_o-\tau_p)u(t+N\tau_o-\tau_p) \\ -\Delta Q_B[t+(N-1)\tau_o]u[t+(N-1)\tau_o]h_N \end{cases}; -N\tau_0 \le t \le -(N-1)\tau_0 \quad (3)$$

where

$$h_N = \begin{cases} 1; N \ge 1 \\ 0; N = 0 \end{cases} \quad (4)$$

and the measured signal is

$$S_{AB}(t) = \sum_{N=0}^{\infty} S_{AB_N}(t) \quad (5)$$

The demodulated signal from the lock-in amplifier is the Fourier transform of the WM-DPTR signal and is expressed as in-phase $\Delta S_{IP}(\omega_o)$ and quadrature $\Delta S_Q(\omega_o)$ channels:

$$S_{IP}(\omega_o) = \frac{2}{\pi} b_1(\omega_o)$$

$$\Delta S_Q(\omega_o) = -\frac{2}{\pi} a_1(\omega_o) \tag{6}$$

with

$$\begin{bmatrix} a_1(\omega_o) \\ b_1(\omega_o) \end{bmatrix} = \frac{\omega_o}{\pi} \int_0^{\tau_o} S_{AB}(t) \begin{bmatrix} \cos(\omega_o t) \\ \sin(\omega_o t) \end{bmatrix} dt \tag{7}$$

which can be described as amplitude V_{AB} and phase P_{AB}:

$$V_{AB} = \sqrt{\Delta S_{IP}^2 + \Delta S_Q^2}$$

$$P_{AB} = \tan^{-1}\left(\frac{\Delta S_Q}{\Delta S_{IP}}\right) \tag{8}$$

2.3 WM-DPTR-Based Alcohol Sensor Calibration

A WM-DPTR alcohol biosensor calibrator has been developed through simulation based on the WM-DPTR theory described in the previous section with the differential amplitude and phase calculated using Eqs. 8. The IR detector bandwidth factor $K(\lambda_1,\lambda_2)$ was set to [illegible] $WK^{-1}cm^{-3}$ and the modulation frequency was set at 90 Hz. The fitting parameter $\bar{\mu}_{ea}$ was varied from 0 to 1000 cm^{-1} to obtain the best fit. This is accomplished by finding the value that gives the minimum mean square error (MMSE) between the calibration curves and ethanol measurement results, optimizing the fitting parameter in the whole range of ~0-100 mg/dL. The optimization could be performed for bundled ranges of interest by the sensitivity tunability property demonstrated in [13]. In the ethanol measurement simulation, the samples, which are solutions with 0-120 mg/dL of ethanol in human blood serum diffused through skin, were considered to be excited using two out-of-phase laser beams of wavelengths 9.5 μm and 10.4 μm. The IR detector band was set to 2-5 μm which is consistent with the detection band of the MCZT detector used in the experimental setup. The lock-in amplifier time constant was set at 10 s and prior transient delay period number N was set to 1000.

Appropriate equations were used to model the optical and thermal properties of the sample. The absorption coefficient of the sample was calculated from [16]

$$\mu_e = \sum_i v_i \mu_{e,i} \tag{9}$$

where $\mu_{eA,i}$ is the absorption coefficient of the pure component i and v_i is the volume fraction of the pure component i. The thermal conductivity was computed from [17]

$$k = \sum_i v_i k_i \tag{10}$$

where k_i is the thermal conductivity of the pure component i. The thermal diffusivity was determined from [18]

$$\alpha = \frac{k}{\rho c} = \frac{k}{\sum_i v_i \rho_i c_i} \tag{11}$$

where ρc is the product of density and specific heat capacity of the sample, ρ_i is the density of the pure component i, and c_i is the specific heat capacity of the pure component i. The components in the model consist of ethanol, blood serum, and skin. 70.2% is used as the volume fraction of water in the dermis in the simulations [19].

Values for the thermal and optical properties of ethanol, water, serum, and skin used in the simulator were drawn from various sources. The ethanol absorption coefficient was obtained from NIST Chemistry WebBook [20], the water spectrum from Wieliczka *et al.* [21],

the thermal properties of ethanol-water from measurements by Wang and Fiebig [22], the thermal properties of skin from Dai *et al.* [23], the optical properties of skin from Michel *et al.* [24], the thermal properties of human serum from data on IT'IS Foundation database [25], and the optical properties of human serum from the work by Giovenale *et al* [26].

The optical and thermal properties of human serum with different ethanol concentrations C_{ETOH} diffused from skin are listed in Table 1. The absorption coefficient μ_{eB} is 1036.5 cm^{-1} for all ethanol concentrations.

Table 1. Optical and Thermal Property Changes with Varying Ethanol Concentration in Human Serum Solutions Diffused through Skin

C_{ETOH} (mg/dL)	μ_{eB} (cm^{-1})	k (10^{-3} W/cm K)	α (10^{-3} cm^2/s)
0	832.1	5.230	1.3231
20	832.0	5.229	1.3230
40	831.9	5.228	1.3229
60	831.8	5.227	1.3229
80	831.7	5.227	1.3228
100	831.6	5.226	1.3228
120	831.5	5.225	1.3227

2.4 Ethanol Concentration Estimation

The developed ethanol concentration estimator uses the ethanol calibration curves to estimate BAC based on both measured amplitude and phase. It takes the weighted average of BAC estimated using measured amplitude, $BAC_{amplitude}$, and phase, BAC_{phase}, to obtain an estimated ethanol concentration. Importantly, it takes advantage of the WM-DPTR amplitude and phase complementary sensitivity to optimize the accuracy and precision of the developed biosensor, as illustrated in Fig. 3. The amplitude of the differential signal has higher sensitivity at low ethanol concentrations and the phase exhibits higher sensitivity at high concentrations. Therefore, more weight is applied to $BAC_{amplitude}$ if the estimated BAC is in the low ethanol concentration range and more weight to BAC_{phase} in the high ethanol concentration range. A threshold value is used to determine these low and high ethanol concentration ranges. Setting the threshold value to 50 BAC gave the best results. The estimated BAC is calculated as follows.

$$Estimated\ BAC = \beta BAC_{amplitude} + (1-\beta) BAC_{phase} \tag{12}$$

3. Results and discussion

Fig. 4 shows the calibration curve with the experimental results when the fitting parameter $\bar{\mu}_{IR}$ is set to 141 cm^{-1} for the best overall fit for both amplitude and phase. After varying β between 0 and 1, it was found that the smallest mean absolute error and mean variance were obtained when setting β to 0.74 for low ethanol concentrations and 0.06 for high ethanol concentrations. As shown in Fig. 4, the calibration curves and experimental ethanol measurement results have similar overall shapes. Both the amplitude and the phase of the differential signal decrease monotonically with increasing ethanol concentration. Table 2 shows the alcohol biosensor performance if the calibration curves in Fig. 4 are used for ethanol concentration estimation. The mean absolute error and mean variance (a measure of biosensor precision) are 0.23 mg/dL and 0.12 mg/dL respectively.

To improve the results, the fitting parameters were optimized separately for amplitude and phase. Fig. 5 shows the calibration results when the amplitude fitting parameter $\bar{\mu}_{IR}$ is set at 174 cm^{-1} for best amplitude fit and the phase fitting parameter $\bar{\mu}_{IR}$ is set at 129 cm^{-1} for best phase fit. In addition, β is set at 0.75 for low ethanol concentrations and at 0.04 for high ethanol concentrations for lowest mean absolute error and mean variance. The ethanol concentration estimation results are shown in Table 3. The mean absolute error and mean variance are 0.19 mg/dL and 0.12 mg/dL, respectively.

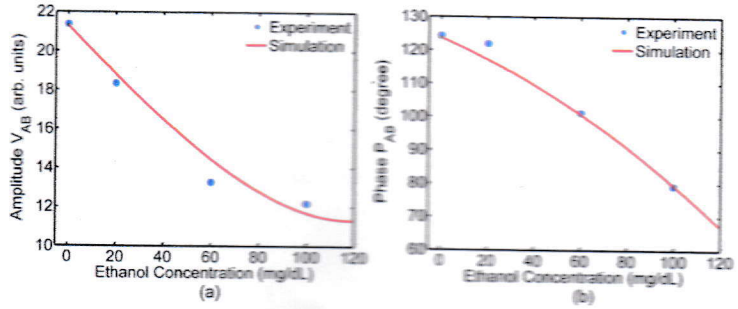


Fig. 4. Ethanol Calibration Curves Using a Common Fitting Parameter Value for Amplitude and Phase with the System Parameter Combination of R = 0.99, dP = 179.68°: (a) Amplitude and (b) Phase

Table 2. Ethanol Concentration Estimation Using a Common Fitting Parameter Value for Amplitude and Phase with the System Parameter Combination of R = 0.99, dP = 179.68°

Actual Ethanol Concentration (mg/dL)	Estimated Ethanol Concentration (mg/dL)	Accuracy (Systematic Error in mg/dL)	Precision (Standard Deviation in mg/dL)
0	0.00	0.00	0.00
20	19.36	0.64	0.35
60	59.98	0.02	0.61
100	99.76	0.24	0.06

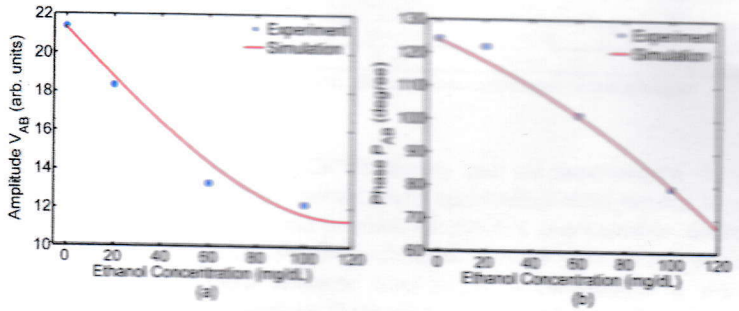


Fig. 5. Ethanol Calibration Curves Using Different Fitting Parameter Values for Amplitude and Phase with the System Parameter Combination of R = 0.99, dP = 179.68°: (a) Amplitude and (b) Phase

Table 3. Ethanol Concentration Estimation Using Different Fitting Parameter Values for Amplitude and Phase with the System Parameter Combination of R = 0.99, dP = 179.68°

Actual Ethanol Concentration (mg/dL)	Estimated Ethanol Concentration (mg/dL)	Accuracy (Systematic Error in mg/dL)	Precision (Standard Deviation in mg/dL)
0	0.00	0.00	0.00
20	19.50	0.50	0.28
60	60.11	0.11	0.63
100	100.13	0.13	0.02

Tables 4 and 5 compare the accuracy and precision of the developed alcohol biosensor with commercial alcohol biosensors in-vitro measurement performance and DADSS specifications. The developed WM-DPTR-based alcohol biosensor exceeds the DADSS specifications in terms of both accuracy and precision for all measured ethanol concentrations. Its accuracy is comparable to other technologies, but its precision can outperform all other technologies for all measured ethanol concentrations. In terms of measurement time, the commercial biosensors can determine ethanol concentration in a time frame on the order of seconds. For ethanol measurements using the WM-DPTR-based biosensor, a large (10 s) time

constant was applied to ensure signal stability since aged lasers were used during the measurement, leading to long delay in lock-in amplifier steady measurements and resulting in a measurement time of about 2 minutes. This record can be vastly improved with state-of-art QCL technology.

Table 4. Comparison with Other Alcohol Biosensors – Systematic Error[a]

		Autoliv [9]	TruTouch [9]	WM-DPTR	DADSS Specifications [9]
Ethanol Concentration	0			0.00	1
	20	0.2		0.50	1
	60			0.11	0.7
	80	0.8	0.1		0.3
	100			0.13	
	120	0.0			1
In-vivo or In-vitro		In-vitro	In-vitro	In-vitro	
Measurement Time		5 sec.	30 sec.	120 sec.	325 ms

[a]Units for systematic error: mg/dL. Shaded areas: Information is not available.

Table 5. Comparison with Other Alcohol Biosensors – Standard Deviation[b]

		Autoliv [9]	TruTouch [9]	WM-DPTR	DADSS Specifications [9]
Ethanol Concentration	0			0.00	1
	20	1.7		0.28	1
	60			0.65	0.7
	80	2.2	1.6		0.5
	100			0.02	
	120	2.7			0.1
In-vivo or In-vitro		In-vitro	In-vitro	In-vitro	
Measurement Time		5 sec.	5 sec.	30 sec.	120 sec.

[b]Units for standard deviation: mg/dL. Shaded areas: Information is not available.

4. Conclusion

A calibration method based on WM-DPTR theory and on experimental data has been introduced to convert the WM-DPTR method into a quantitative ethyl alcohol biosensor. The calibrated biosensor exhibits very-good-to-excellent alcohol concentration accuracy in the case of ethanol and human serum solutions diffused through skin: it can achieve a high accuracy of 0.19 mg/dL in mean absolute error which is comparable to state-of-the-art commercial non-invasive ethanol sensors. Furthermore, it outperforms other alcohol detection technologies in terms of precision, achieving a high precision of 0.02 mg/dL in mean variance. If best-fits of the experimental data to WM-DPTR theory are done separately for amplitude and phase, they result in better fitting between calibration curves and experimental results, thereby improving the performance of the biosensor. It is expected that the ethanol measurement time using the WM-DPTR-based biosensor will decrease substantially with state-of-the-art quantum cascade lasers.

Acknowledgements

The authors wish to acknowledge the Natural Sciences and Engineering Research Council of Canada (NSERC) for financial support of this research project through Engage and Discovery grants to AM.